ARL-TR-9185 • APR 2021

Exploration of Ground Obstacle Visibility in a Degraded Visibility Environment by an Airborne Landing Radar

by Christopher S Kenyon

NOTICES

Disclaimers

ARL-TR-9185 ● APR 2021

Exploration of Ground Obstacle Visibility in a Degraded Visibility Environment by an Airborne Landing Radar

Christopher S Kenyon
Sensors and Electron Devices Directorate, DEVCOM Army Research Laboratory

REPORT DOCUMENTATION PAGE	*Form Approved* *OMB No. 0704-0188*

1. REPORT DATE *(DD-MM-YYYY)*	April 2021
2. REPORT TYPE	Technical Report
3. DATES COVERED (From - To)	30 September 2019–8 March 2021
4. TITLE AND SUBTITLE	Exploration of Ground Obstacle Visibility in a Degraded Visibility Environment by an Airborne Landing Radar
5a. CONTRACT NUMBER	
5b. GRANT NUMBER	
5c. PROGRAM ELEMENT NUMBER	
6. AUTHOR(S)	Christopher S Kenyon
5d. PROJECT NUMBER	R.0041090.5
5e. TASK NUMBER	
5f. WORK UNIT NUMBER	
7. PERFORMING ORGANIZATION NAME(S) AND ADDRESS(ES)	DEVCOM Army Research Laboratory ATTN: FCDD-RLS-RM 2800 Powder Mill Rd Adelphi, MD 20783
8. PERFORMING ORGANIZATION REPORT NUMBER	ARL-TR-9185
9. SPONSORING/MONITORING AGENCY NAME(S) AND ADDRESS(ES)	
10. SPONSOR/MONITOR'S ACRONYM(S)	
11. SPONSOR/MONITOR'S REPORT NUMBER(S)	
12. DISTRIBUTION/AVAILABILITY STATEMENT	Approved for public release: distribution unlimited.
13. SUPPLEMENTARY NOTES	ORCID ID: Christopher S Kenyon, 0000-0003-1209-8335

14. ABSTRACT

Computed 3-D 35-GHz radar images from a proposed forward-looking synthetic aperture radar (SAR) are shown to help evaluate a proposed landing radar that would mount on the front of a helicopter. The radar, which is currently under design at the US Army Combat Capabilities Development Command Army Research Laboratory, would assist landing in degraded visual environments. In particular, 3-D SAR images of three near-ground obstacles—an overhead power-line section and a pristine ZSU antiaircraft vehicle, both over flat ground, and a boulder field—are created from computed radar data from their models. SAR images of the models shown in a 3-D space are clearly visible, though the power line may only be detected at very limited incidence angles. Boulders over a rough ground were clearly distinct even with a ground roughness characterized by a root-mean-square height of 15 cm with a correlation length of 2 m.

15. SUBJECT TERMS

radar, 3-D SAR, 3-D images, degraded visual environment, DVE, helicopter, flight path, landing obstacles, Xpatch, Matlab, ParaView, rough ground

16. SECURITY CLASSIFICATION OF:			**17. LIMITATION OF ABSTRACT**	**18. NUMBER OF PAGES**	**19a. NAME OF RESPONSIBLE PERSON**
a. REPORT	**b. ABSTRACT**	**c. THIS PAGE**			Christopher S Kenyon
Unclassified	Unclassified	Unclassified	UU	58	**19b. TELEPHONE NUMBER (Include area code)** (301) 394-5547

Standard Form 298 (Rev. 8/98)
Prescribed by ANSI Std. Z39.18

Contents

List of Figures

List of Tables

1. Introduction

Army helicopters in arid climates are at times confronted with dust storms near the ground. If they need to land in such conditions, they need to be able to see the ground and any obstacles within the vicinity of the possible landing site that could interfere with the landing. Airborne dust in such a degraded visibility environment (DVE) is likely to render normal optical means inadequate.

As an alternate to those normal visual means, the Army is working on a radar system that would reside on the front of a helicopter to effectively see through the dust.[1] This report presents some preliminary results, from computer modeling, of radar imaging at about 35 GHz with a 500-MHz bandwidth of some possible targets or objects on or near the ground that could be of interest or concern to a pilot attempting a landing in a DVE.

Our primary radar return computation tool is the shooting-and-bouncing ray (SBR) radar return computation software Xpatch,[2] now being maintained and enhanced by Leidos. We postprocess the signal signatures from Xpatch with Matlab using the back-projection algorithm into 3-D image files that we display as 3-D images.

We have chosen to model radar returns of three separate objects that might pose a problem for a landing helicopter. The objects are a power-line cable, a detailed ZSU antiaircraft model,[3] and a boulder field. The main goal, given the constraints on a suitable helicopter-mounted radar, is to see how well those returns can be presented in real, or near-real, time as image information to pilots flying that aircraft. In this report, we show snapshots of computed 2- and 3-D radar images of the three objects resulting from the modeling and Xpatch computations.

In the methodology section, we discuss how we get there. In the results section, we discuss and show the results. The final section provides the conclusion and discusses further work.

2. Methodology

2.1 About the DVE Radar

In our modeling, a DVE helicopter landing radar is equipped with a 2-m-wide bumper-style antenna array that provides an about 0.8° aperture for resolution in the azimuth for a distance to target of 150 m.

This report assumes, for the computer modeling, that the radar transmitters and receivers will take a horizontal straight path over the ground toward a proposed landing site. It may take several such horizontal paths in a stair-step-type descent to acquire the data for the imaging. We assume that in-flight aberrations from that straight path and the orientation of the radar antennas could be compensated for by inertial guidance devices and computer processing. For our calculations, the radar is looking at a point ahead on the ground while the helicopter travels forward horizontally for 15 m, so that the look-down angular spread, or aperture, spanning 9.4° to 10.4° in elevation constitutes a vertical aperture of 1° for each image following the radar example in Dogaru.[1] Figure 1 illustrates how the vertical aperture is acquired from this kind of approach to a possible landing site. A 2-m width of the radar antennas across the face of the helicopter provides an aperture in the cross direction of about 0.8° at a 150-m distance from the landing site.

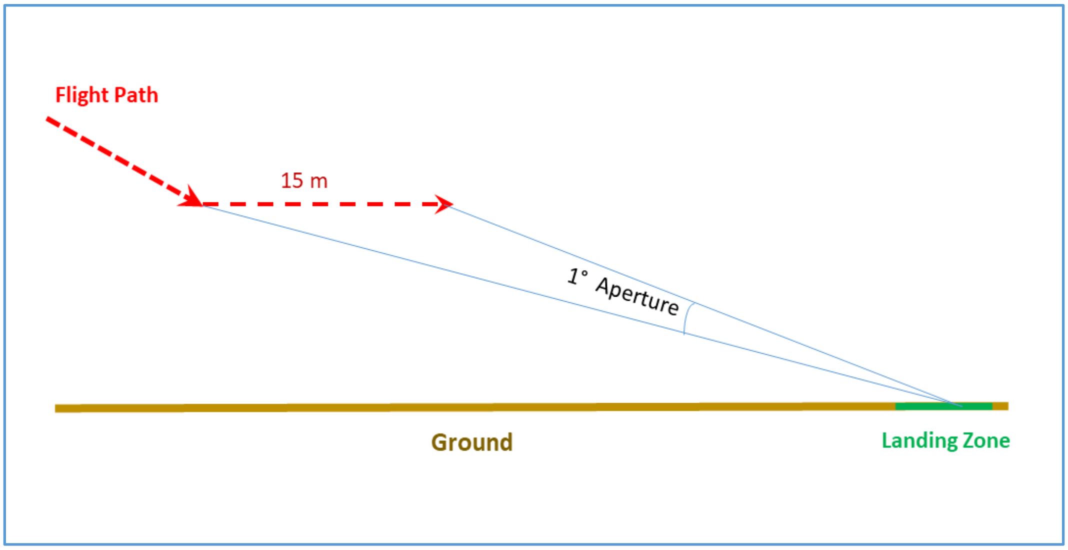

Fig. 1 Vertical aperture acquired from flight path

The radar frequency used was a band from 34.7 to 35.2 GHz. Such high frequencies required a very high number of radar return computations per unit area and consequently necessitated the use of Xpatch as it provides a very fast, but approximate, SBR approach.

The 0.5-GHz bandwidth (B) limits the depth or downrange resolution to c/(2B) = 0.3 m. The cross-range resolution in the x-direction is limited by the aperture that the antenna width presents. We can use a couple relations to obtain this approximate cross-range resolution. With an effective bandwidth of $B_x \approx f_c\, \theta_{int}$[4] and cross-range resolution of $\Delta CR_x = c/(2B_x)$, with an integration angle of θ_{int}, of 0.8° and center radar frequency, f_c, of 34.95 GHz, we obtain $\Delta CR_x \approx 0.31$ m. The radar's z-cross-range resolution, ΔCR_z, with an aperture of 1° while the helicopter is still looking down at about 10° is then ≈ 0.25 m.

2.2 The Object Models

The modeling starts with a CAD model of an object that we have obtained from various sources. The power-line cable model was created at the US Army Combat Capabilities Development Command Army Research Laboratory using FEKO CAD software[5] and parameters for a seven-strand power-line cable in a paper by Sarabandi and Park.[6] The ZSU model was developed by the Ballistic Research Laboratory. The boulders were from the Army Model Exchange.[7] All of the models were already in triangular surface facet format except for the power-line cable. The cable model was converted from the stl format exported by FEKO into an ACAD facet file format required by Xpatch using ModelMan software.*

The CAD model consists principally of triangular "facets" that describe or represent the surfaces of the objects and the ground in discrete patches. In addition to the facet files of the objects, Xpatch takes in material electrical properties as well, so that dielectrics both on surfaces and in object volumes, including a variety of things in the space of interest, can be properly modeled. The cable was modeled purely as a conductor, as was the ZSU. The boulders were modeled as dielectrics, as were the grounds. The models were also computed for the free-space case without a ground.

The twisted power line comprises seven strands of 4-mm-diameter copper strand with an overall diameter of 12 mm, a pitch of 146 mm, and a length of 19.5 mm axial distance between strands. Figure 2 shows a FEKO image of the end of a power-line section. For this report, a 6.4-m-long piece was modeled over the X-axis horizontally 3 m above a realistic ground as shown in Fig. 3. Although modeled on a catenary, it is only mildly curved because of its limited length.

Fig. 2 End view of FEKO CAD model of a twisted power-line section

*ModelMan was last developed by SAIC to support facet file conversion.

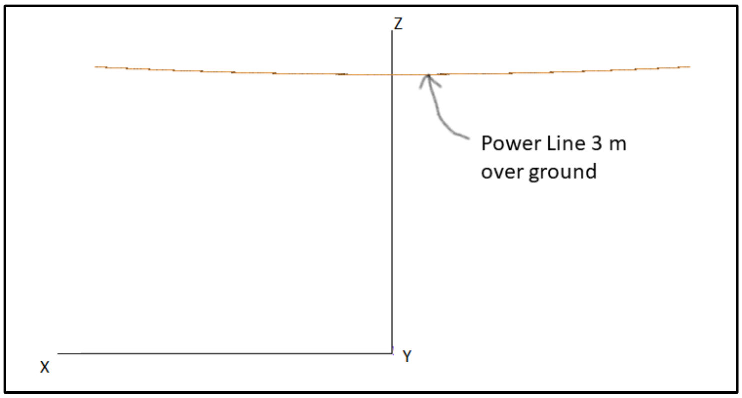

Fig. 3 Snapshot of power-line model over the X-axis

The 120 m-in-X and 150 m-in-Y ground plane for this Xpatch model used a flat earth with a complex permittivity of $\mathrm{Re}\{\varepsilon_r\} = 4.6$ and $\mathrm{Im}\{\varepsilon_r\} = -1.8$. Figure 4 shows a section of the final facet model with the twisted strands used in Xpatch.

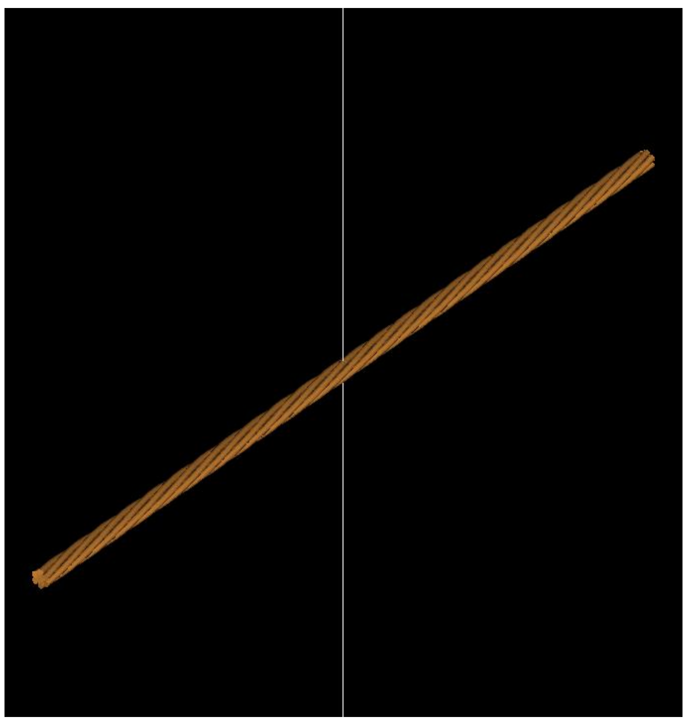

Fig. 4 Facet model of a short section of the twisted-strand power line

Figure 5 shows the ZSU facet model. Its model is pristine in the sense that it is without small flaws or irregularities typically resulting from wear and tear. As such, certain radar returns can be exaggerated or atypical. It is about 6 m long by 3.5 m high, including its radar dish, and about 3 m wide. It was modeled over the X-axis as shown in Fig. 5. We used a 40 × 60 m flat earth with the complex permittivity of (4.6, –1.8) for this model.

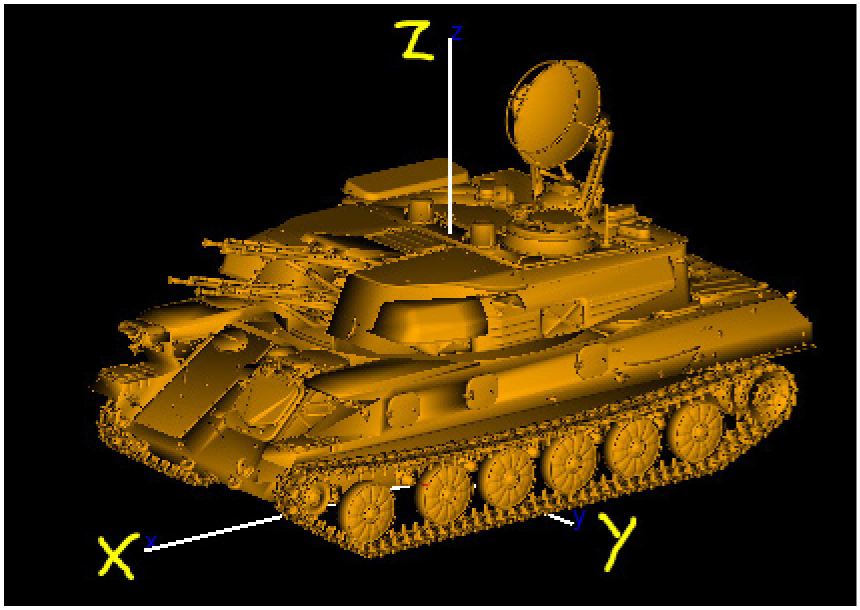

Fig. 5 ZSU facet model aligned with the X-axis

The final objects of concern for a helicopter landing in a DVE that we report on here is a field of five boulders of three types: a 16-, 19-, and 36-inch boulder over a flat earth as shown in Fig. 6. To get a rough idea of the boulder sizes, Table 1 provides the dimensions of boxes that would bound the boulders. Both the boulders and the 40 × 60 m flat earth for this model were given the complex permittivity of (4.8, –1.8) in the Xpatch modeling.

After computing SAR returns for boulders over a flat earth, we computed SAR returns for the boulder field over several rough grounds. Xpatch models rough grounds by randomizing its bumps constrained by user-set root-mean-square (RMS) heights and respective correlation lengths. We looked at RMS heights of 1, 3, 6, 10, and 15 cm, all with correlation lengths of 2 m.

Table 1 Boulder dimensions

Boulder	ΔX [m]	ΔY [m]	ΔZ [m]
16-inch	0.42	0.42	0.30
19-inch	0.46	0.48	0.19
36-inch	0.92	0.46	0.48

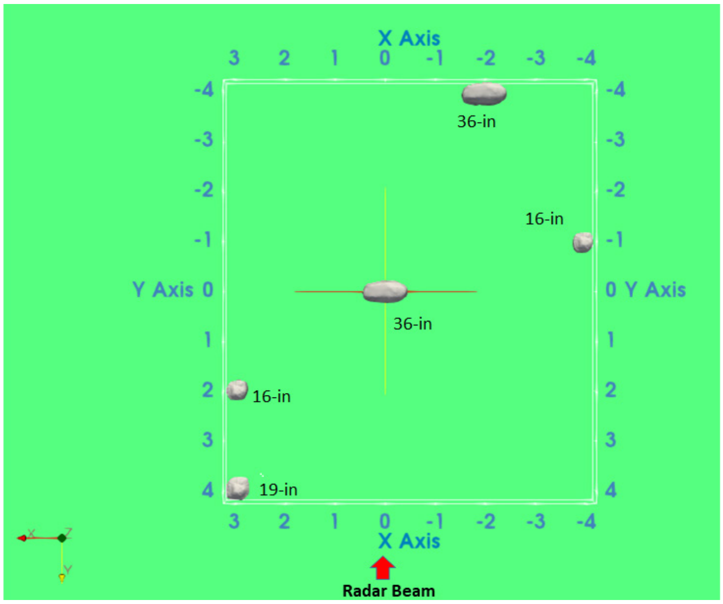

Fig. 6 Boulder field in meters

2.3 Modeling

In this report, we use a right-handed coordinate system with increasing azimuth angle as it opens from the X-axis toward the Y-axis, as shown in Fig. 7, so that it starts from 0° at the X-axis and reaches 90° at the Y-axis. Xpatch software, to the contrary, uses azimuth angles decreasing when moving in the direction from the X- to Y-axis. In the Xpatch modeling for this report, our apertures for azimuth and elevation compelled collection of Xpatch radar return data at azimuths spanning ±0.4° about the primary azimuth directions of interest and ±0.5° about 9.9° of elevation.

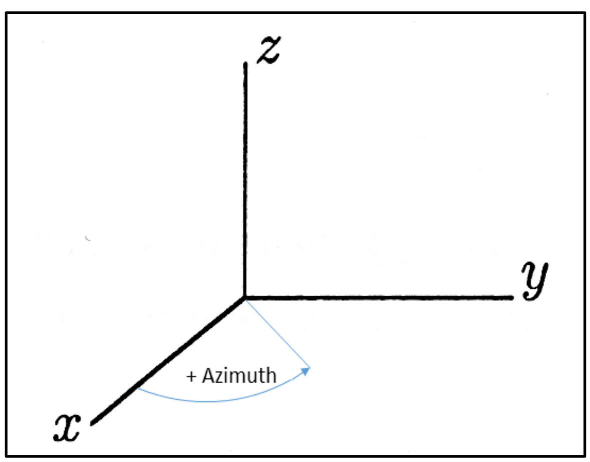

Fig. 7 Increasing azimuth direction used in this report

The facet model is then used with Xpatch high-frequency radar software, which computes the far-field radar return, or "synthetic signal" (ss), data for objects either with a realistic ground or in free space using a SBR algorithm. Since we have three apertures in the Xpatch radar return computations (namely, the azimuth, or horizontal; the elevation, or vertical; and the frequency band width, or depth), our Xpatch data has the information to span a 3-D image space.

From the radar return data, we can create 2-D images, 3-D images (or slices from it), or even 1-D results. We have taken three different routes to get SAR radar images. The fastest route we have taken is to convert the ss data into a trace file using Xpatch output processing software and then feed that into one of its SAR image creation applications, namely, Catalus, to generate a 2-D SAR image. The second route starts with the conversion of the ss data into Matlab "sdata" files, as we have termed them. Then with a Matlab SAR image creation script using a back-projection algorithm created at the DEVCOM Army Research Laboratory, we create a Matlab 3-D image file. From the image file, we can create slices of the 3-D images with Matlab, though they are not shown in this report. For the third route, we converted the Matlab image files to vtk files using a Matlab script. These vtk files are imported into ParaView[8] to display 3-D images with views that can be easily manipulated with a mouse or numerically tuned in roll, elevation, or azimuth. For viewing these 3-D images in other than from the radar direction, the images help to convey the location of the radar return sources rather than what they would look like to the observing radar.

In the creation of the Matlab image files, we applied a Hanning window filter on both the azimuth, or horizontal aperture, and the elevation, or vertical aperture. This filter processing tends to reduce the side bands and noise in the ParaView images relative to images without it.

3. Results

The principal results we show here are from Xpatch's Catalus application for 2-D images and ParaView for 3-D images. The ParaView images are largely a variant of the 3-D image slices that Matlab produces in the sense that ParaView, with its 3-D feature, can usefully display more than just a few slices at a time. The Matlab postprocessing makes it easier to select the image area or volume from the original Xpatch data to eliminate ambiguities appearing on the edges of the computed images in ParaView. In the case of Catalus, the Xpatch app, Cifer, can accomplish some of the same or similar postprocessing of the original Xpatch ss file output prior to their display.

A conductive or perfect electric conductor (PEC) sphere in free space has a well-known radar cross section (RCS) given by πa^2, when $2\pi a \gg \lambda$, where a is the radius of the sphere and λ is the radar wavelength. As such, it can be used as a kind of calibration target. We computed the radar return using Xpatch for a 0.25-m radius PEC sphere in free space with Xpatch to process into images as we have our other targets. By the analytic formula, it should ideally have a RCS of –7.07 dB. The peak RCS for this sphere in our images derived using the Xpatch calculations gives us a rough idea of how much the peak magnitudes in our images may differ from the actual case.

Figures 8 and 9 are SAR images of the PEC sphere rendered by the Catalus and ParaView software, respectively. The peak pixel value in the 2-D Catalus case was –12.2 dB, while the peak voxel value in ParaView was –24 dB. It is clear that these values are significantly lower than the theoretical value of –7.07 dB and it is the case that the images are not calibrated in an absolute sense. However within a given type of SAR representation (e.g., Catalus or ParaView), the sphere case may yield a guide of what to expect for peak SAR for other objects. What is important is the relative magnitude of the return for an object of interest compared to clutter or noise within a given type of representation.

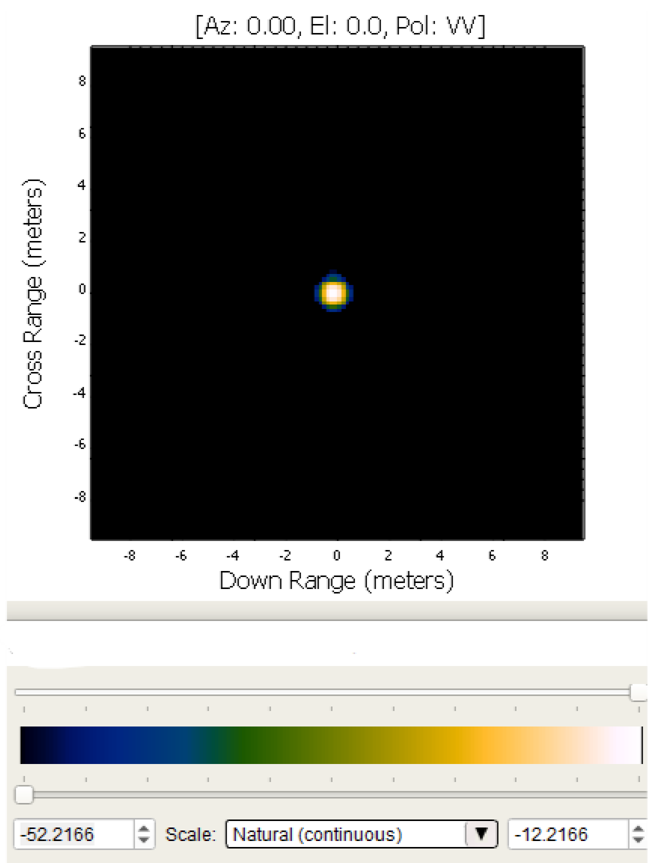

Fig. 8 **Catalus SAR image (dB) of 0.25-m radius PEC sphere in free space**

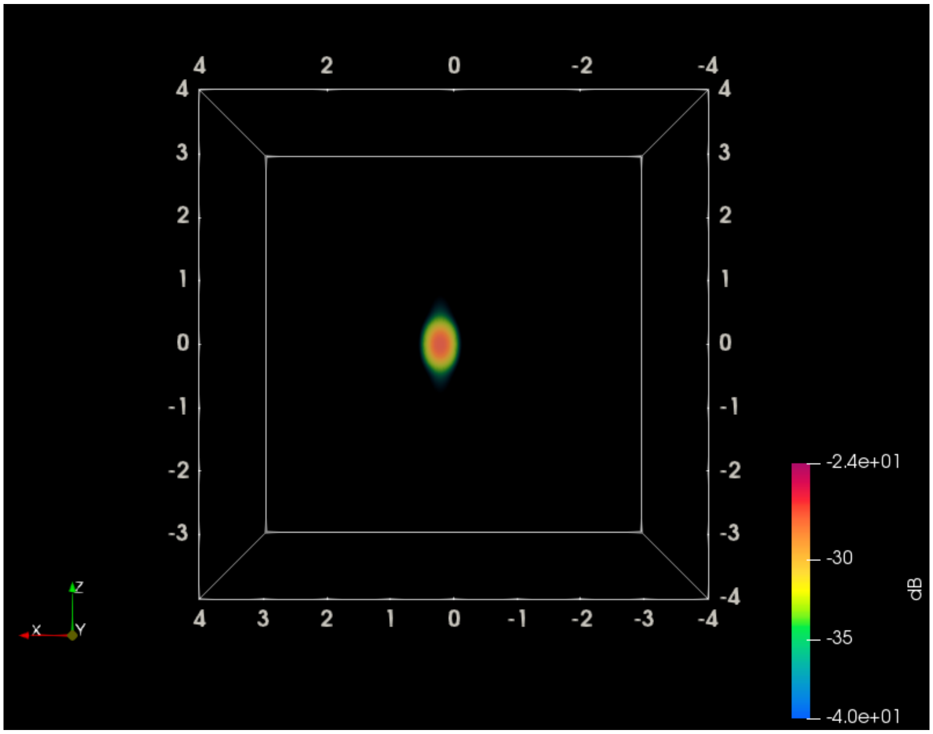

Fig. 9 ParaView (3-D) SAR free-space image of 0.25-m radius PEC sphere

3.1 Seven-Strand Twisted Power Line

Figures 10 and 11 capture the distinct characteristics of the twisted power-line RCS as computed by both the exact method of moments algorithm of FEKO and the more approximate Xpatch, respectively. The results guided azimuthal sampling for the SAR imaging. Figures 12 through 28 show SAR radar images of the 2-m section of twisted strand power-line cable in either free space or suspended 3 m above ground. Free-space images are stated as such in the captions. The figures alternate between Xpatch's Catalus SAR images and ParaView images and show returns for either vertical-vertical (VV) or horizontal-horizontal (HH) polarization. The Catalus images are 2-D SAR images and represent a horizontal slice of the 3-D data with the radar beam incident from the left in the figures. A magenta overlay of the cable facet model is present in the Catalus images when available. In the ParaView images, an overlay of the cable facet model is shown as a thin whitish line usually running through the hotspot of the radar image. As the radar incidence upon the cable turns in azimuth from nearly normal incidence, 89.6°, to 74.6°, the tiny facet line rotates by that 15° difference in the corresponding Catalus SAR images. Following the Catalus images are ParaView images that are intending to reproduce and compare with the corresponding Catalus image with its top-down viewpoint with radar incidence from the left. There is considerable agreement between the images, though the sensitivity between the two varies. ParaView has multiple ways to display the radar images that are composed of bins or voxels. We have mostly used the smoothed-out representation, but in a few cases we used a tetrahedron one as in Fig. 17.

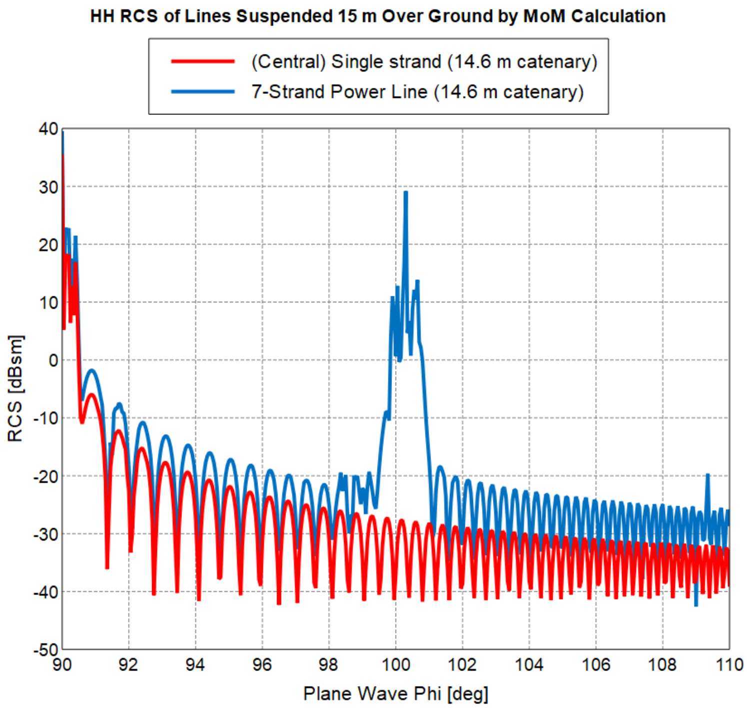

Fig. 10. **HH RCS for single strand vs. six twisted strands at 35 GHz**

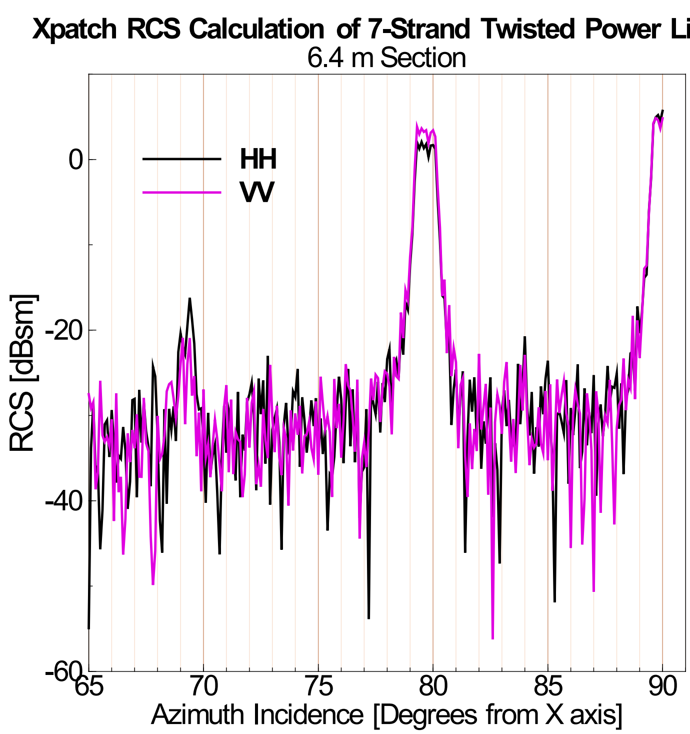

Fig. 11 **Xpatch computed RCS of power line for both VV and HH polarizations**

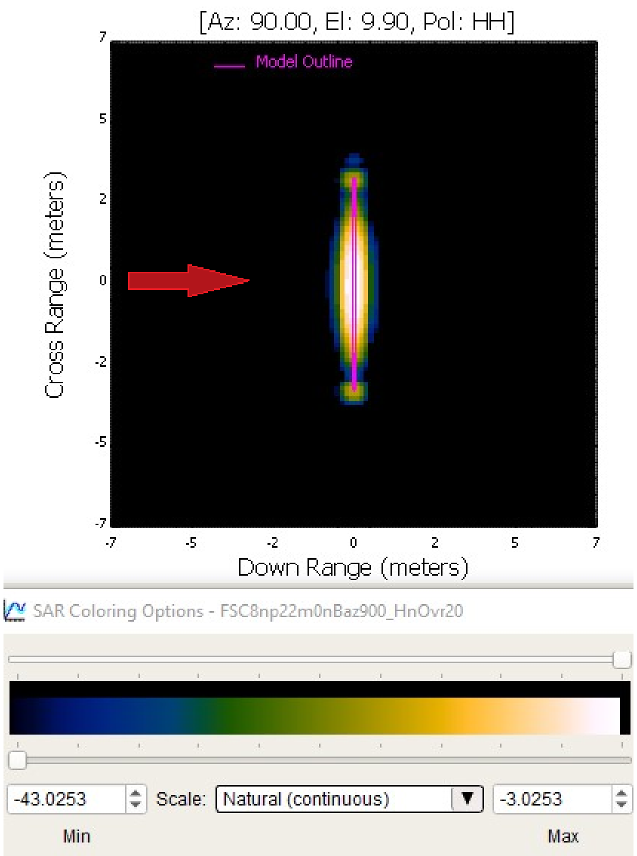

Fig. 12 Catalus 89.6° azimuth-incidence (inc) HH SAR image (dB) from twisted line in free space with radar from left

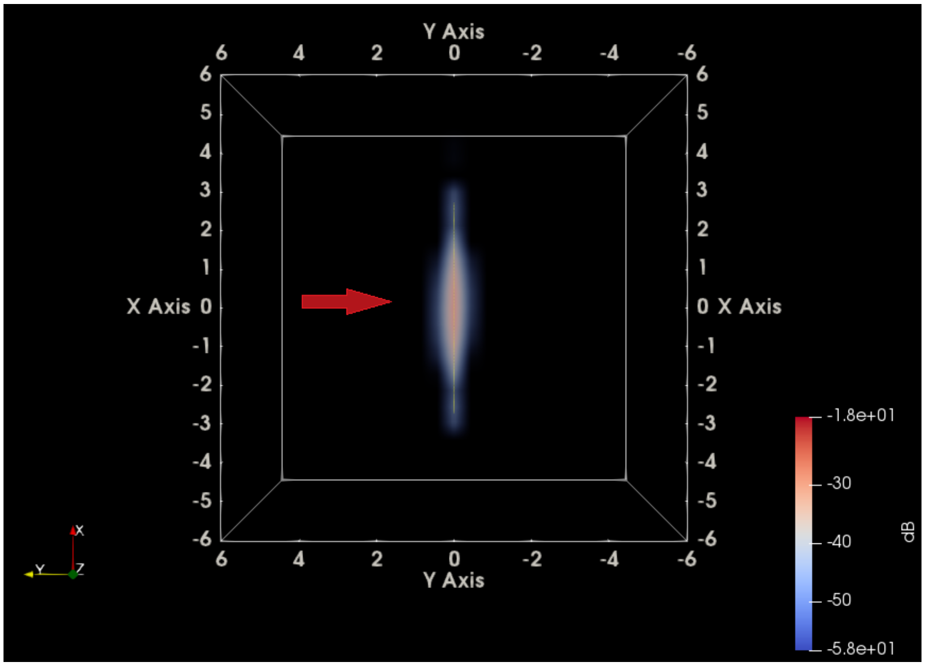

Fig. 13 ParaView top-view 89.6° azimuth-inc HH image from twisted line (overlaid) in free space with radar from the left

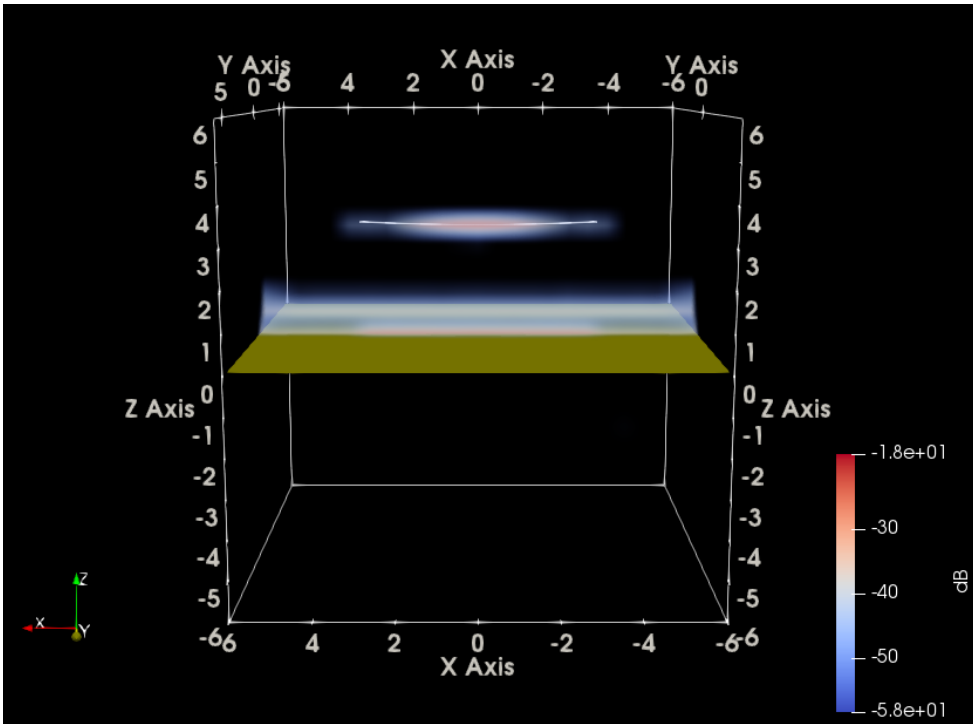

Fig. 14 ParaView 89.6° azimuth-inc HH radar-view image from twisted line (overlaid) over ground

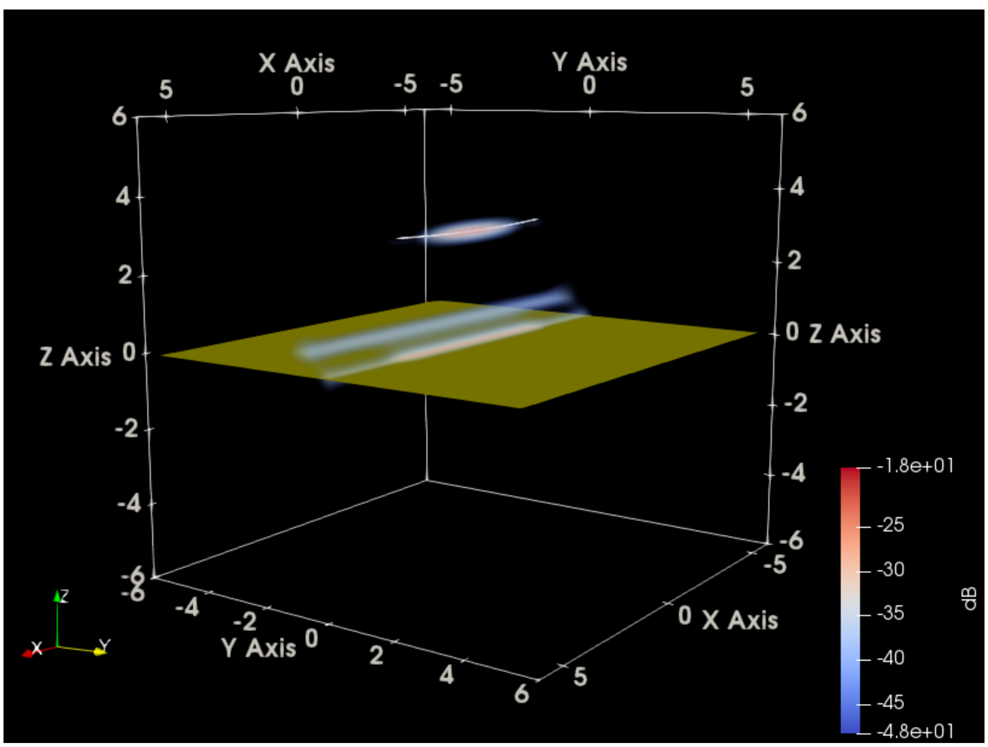

Fig. 15 ParaView 89.6° azimuth-inc HH image from twisted line in side perspective

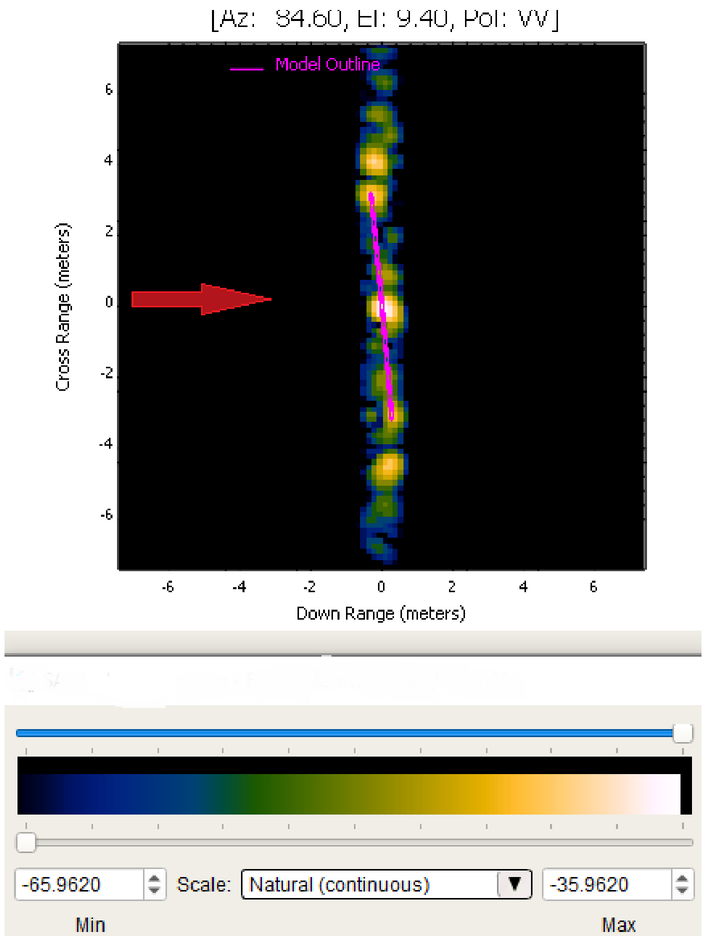

Fig. 16 Catalus HH image (dB) of free-space twisted line at 84.6° azimuth-inc with radar incident from the left

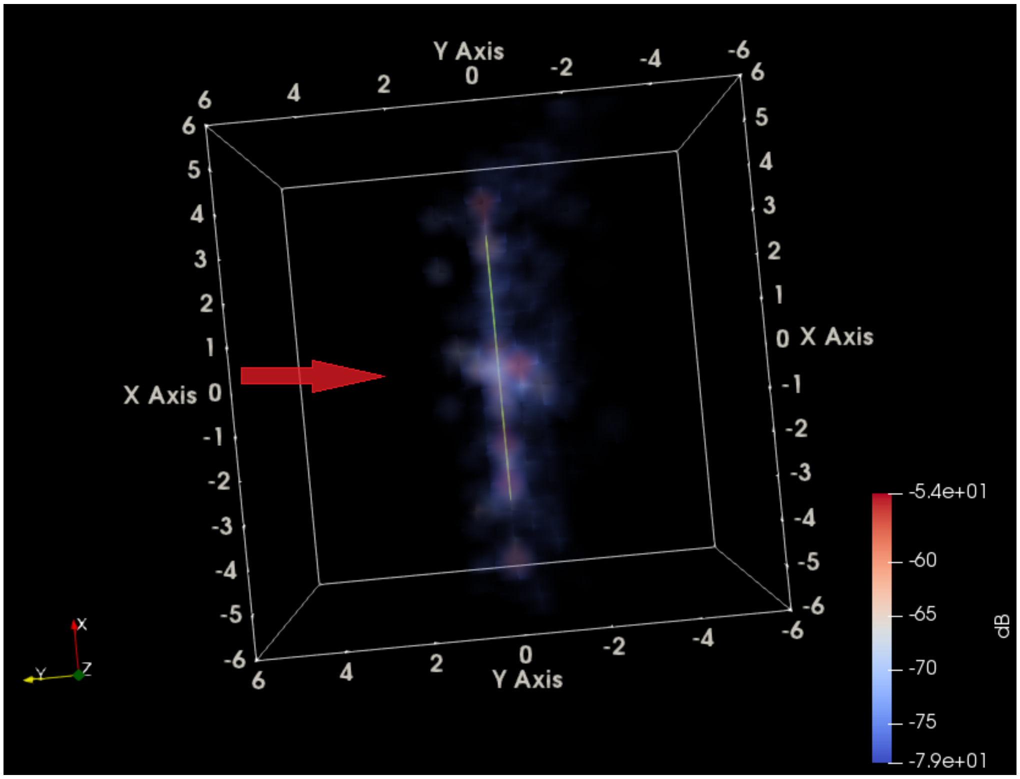

Fig. 17 ParaView top-view HH image of twisted line over ground at 84.6° azimuth-inc with radar incident from the left

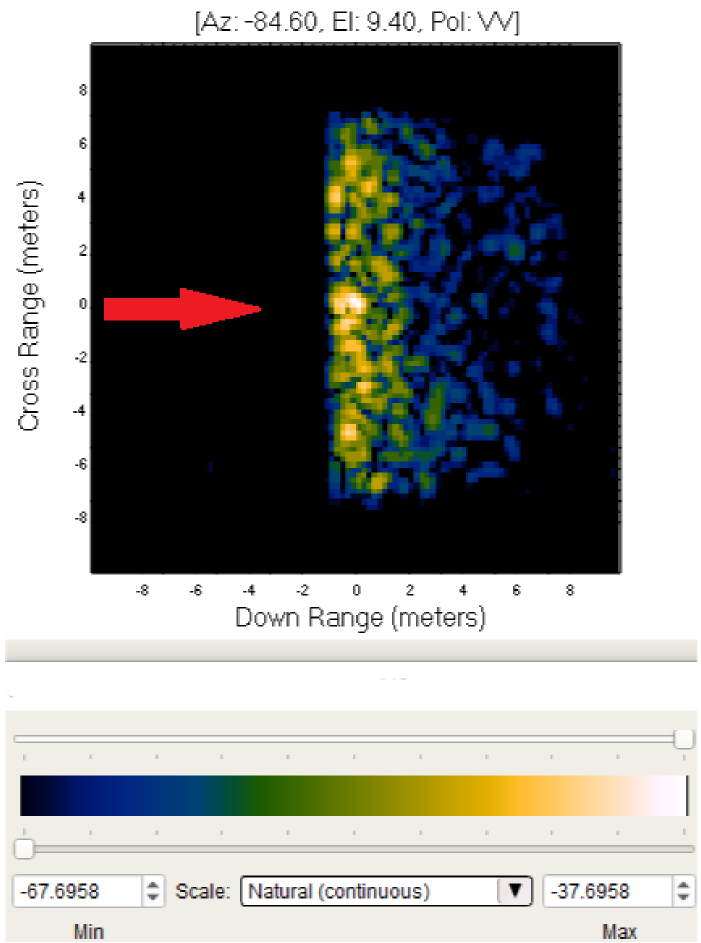

Fig. 18 Catalus VV SAR image of twisted line at 84.6° azimuth over ground

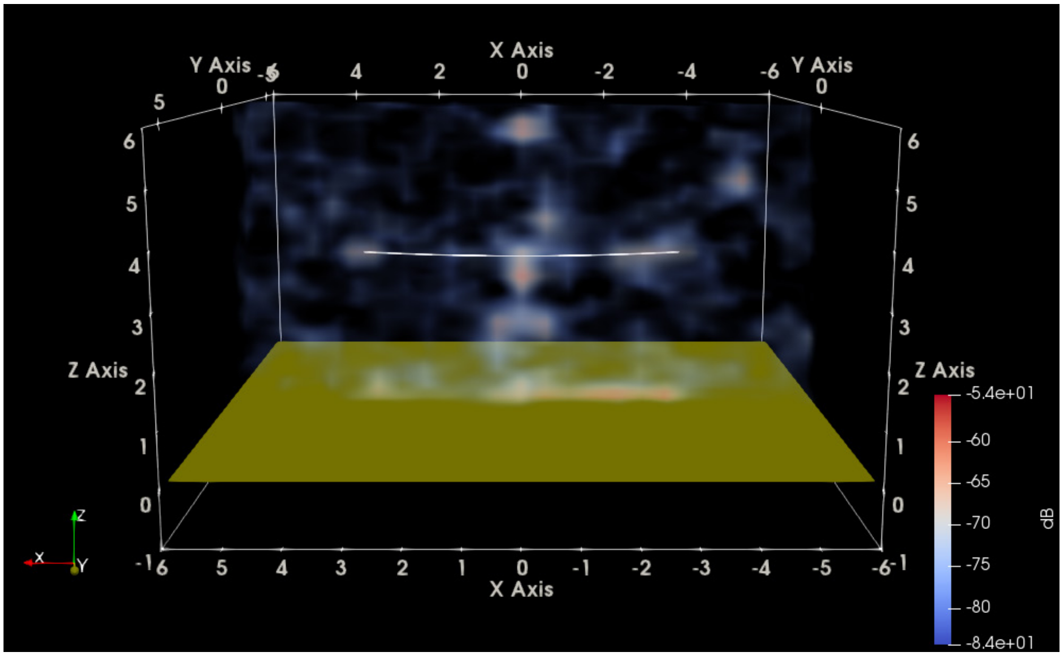

Fig. 19 ParaView radar-view HH image of twisted line at 84.6° azimuth with wire and ground plane overlaid

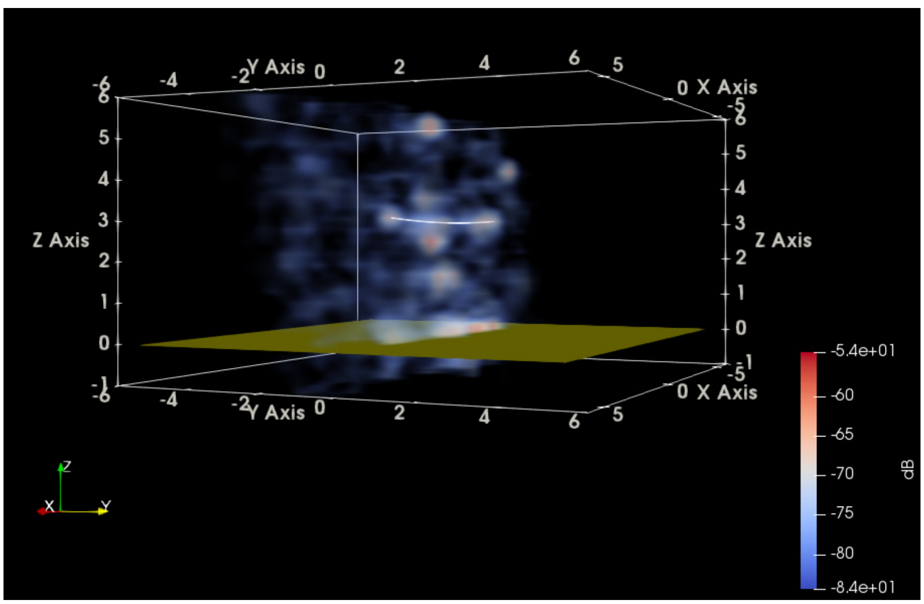

Fig. 20 ParaView VV image of twisted line at 84.5° azimuth side view

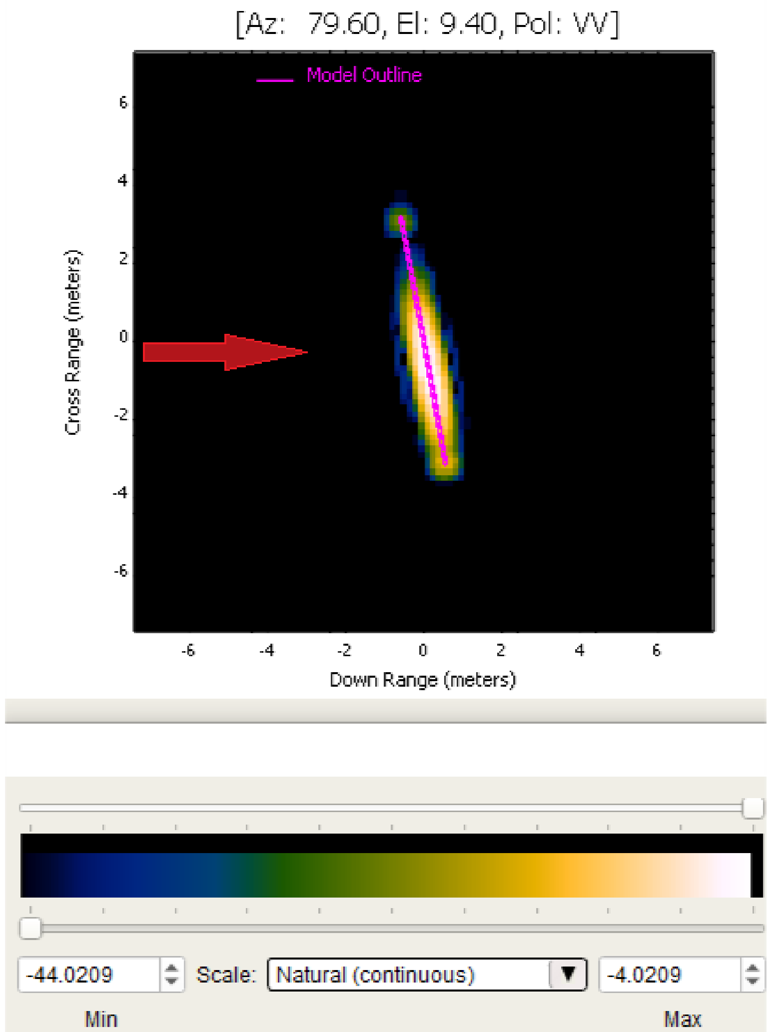

Fig. 21 Catalus VV SAR image (dB) of free-space twisted line at 79.6° azimuth with radar from left

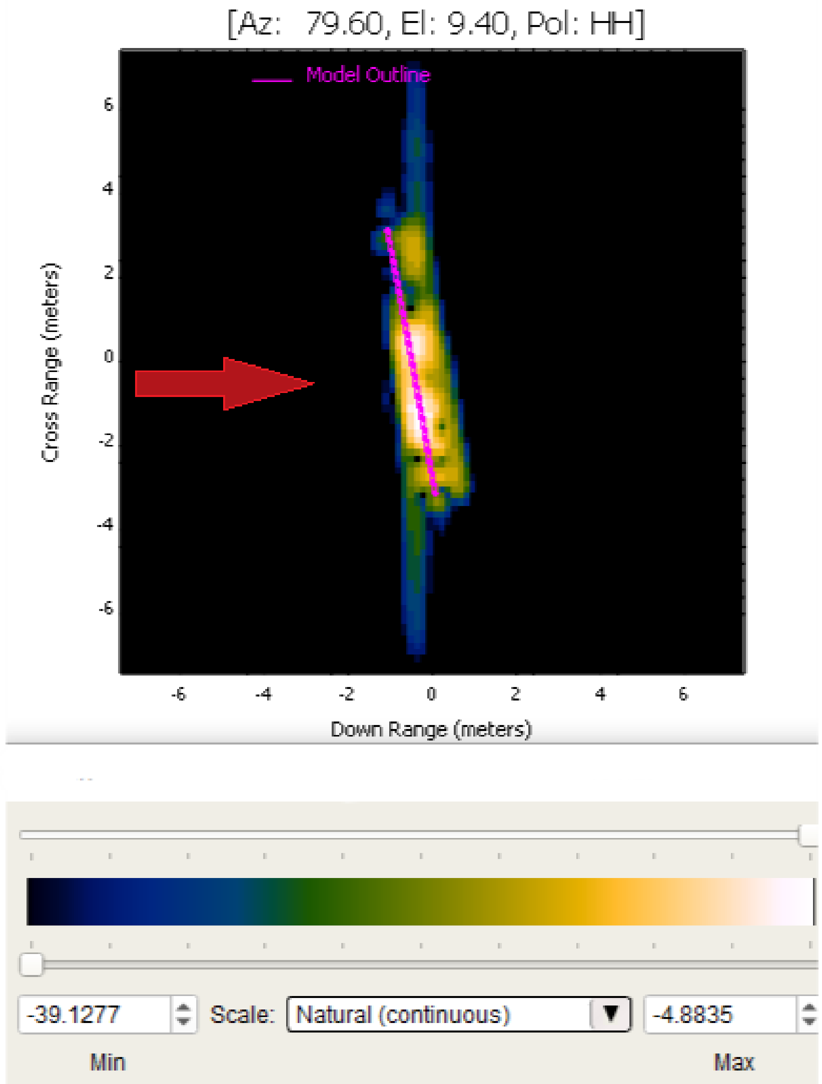

Fig. 22 Catalus HH SAR image (dB) of twisted line over ground at 79.6° azimuth with radar from left

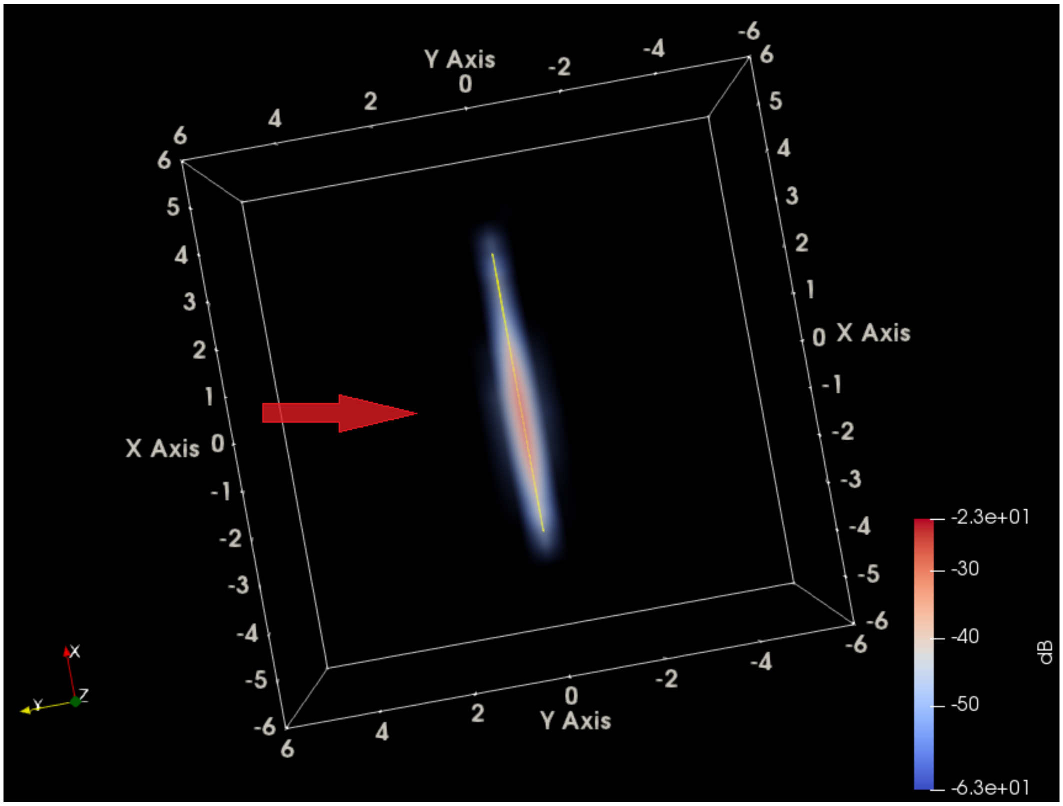

Fig. 23 ParaView HH image of twisted line at 79.6° azimuth-inc, top down, tilted toward radar

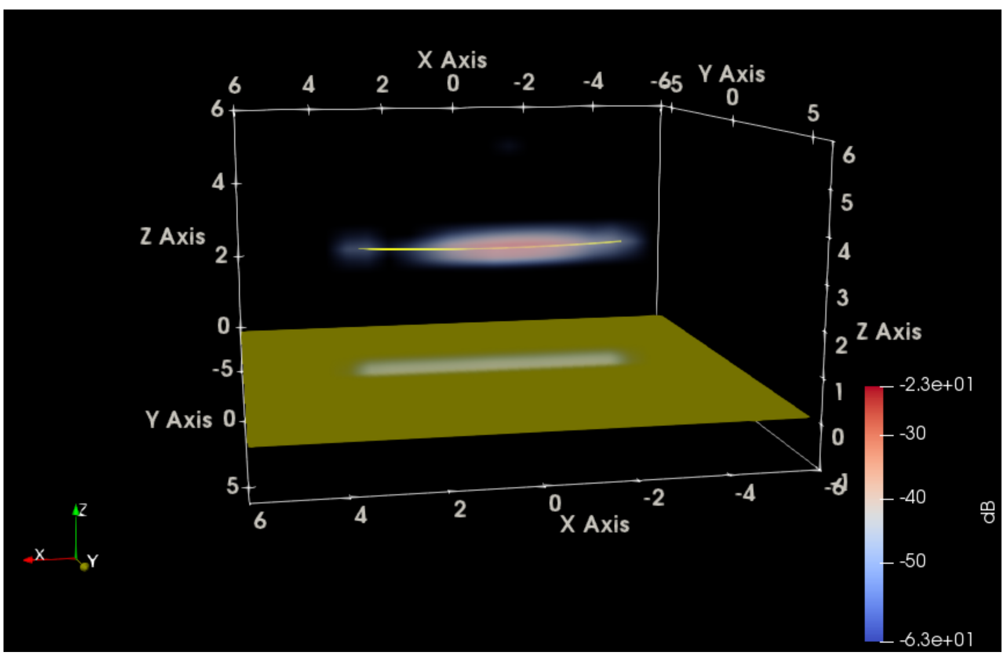

Fig. 24 ParaView HH image of twisted line at 79.6° azimuth, radar view

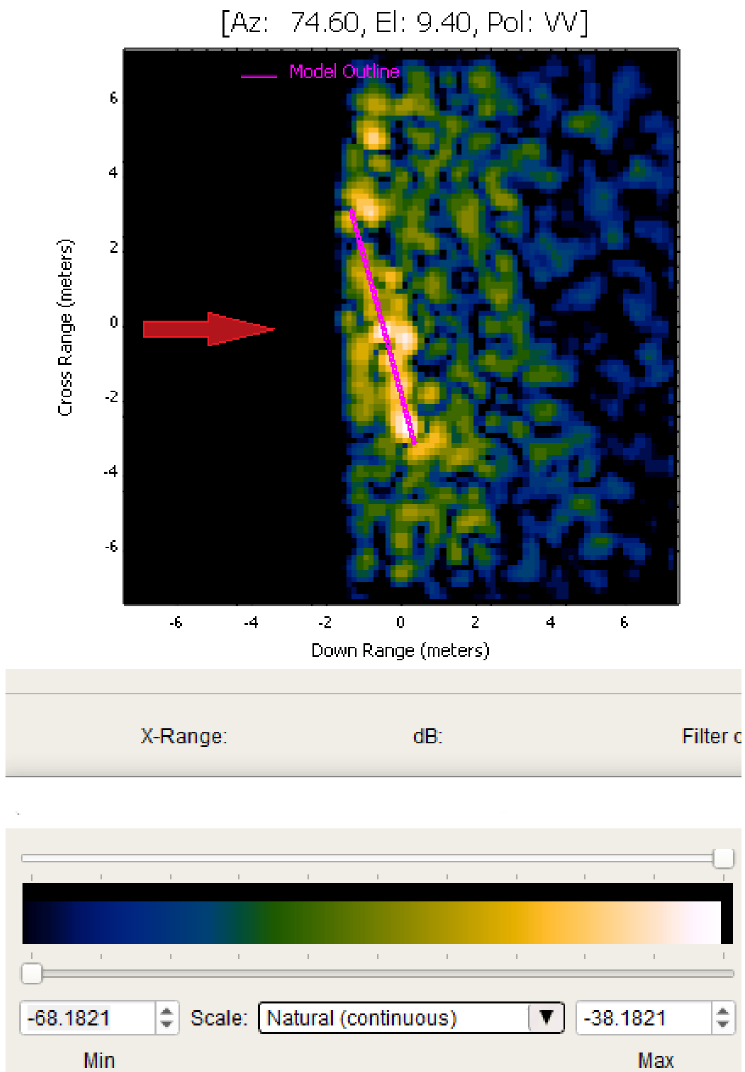

Fig. 25 Catalus VV SAR (dB) of twisted line over ground at 74.6° azimuth-inc

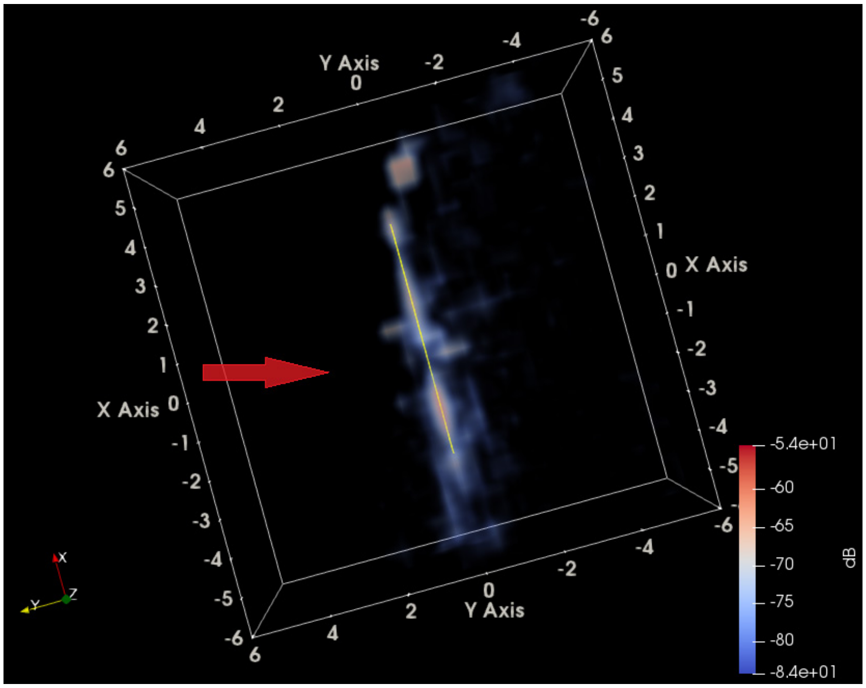

Fig. 26 ParaView HH SAR of twisted line over ground with 74.6° azimuth-inc, top down

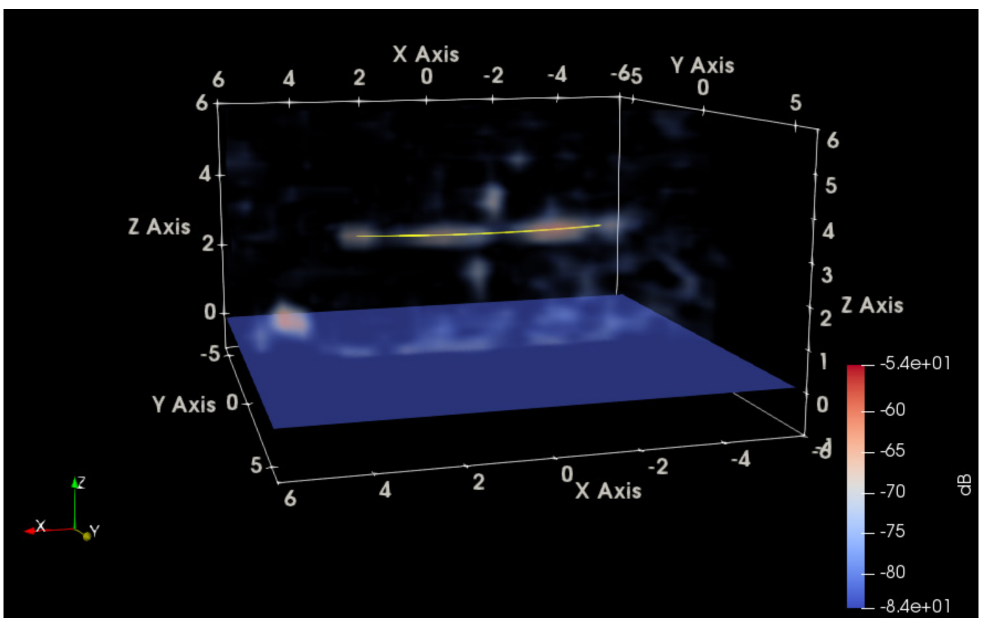

Fig. 27 ParaView HH image of twisted line over ground at with 74.6° azimuth-inc, radar view

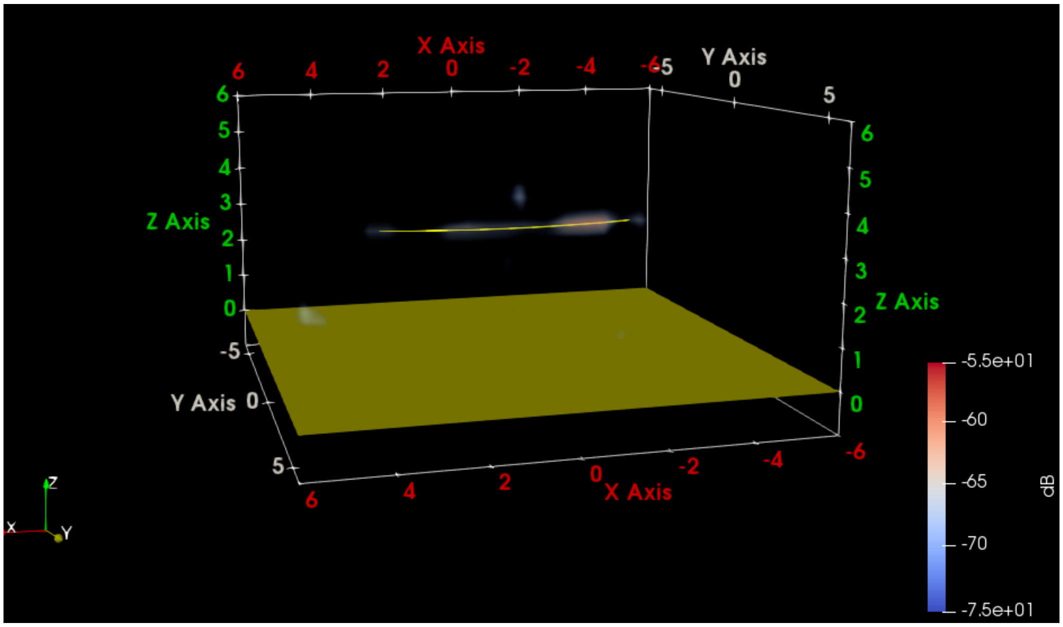

Fig. 28 ParaView VV image of twisted line at 74.6° azimuth-inc, radar view

Since the ParaView images are 3-D, they can be viewed from arbitrary directions to get a better sense of where the strongest returns are coming from. In Figs. 14, 19, 24, 27, and 28, the 3-D images have been rotated by azimuth and elevation to match what the monostatic radar would see for those incidence angles. If one were to process actual radar data by the same algorithms that we are using with Matlab and ParaView here to process our computed ss data, one might choose to default to this monostatic direction. If one wanted the human viewer to more quickly sense depth within the 3-D image, two images of this same data separated slightly in azimuth could be created with each sent to a separate eye via a stereo viewer.

The twisted-strand power-line radar return differs from a non-twisted line by the presence of a spike at several degrees from normal incidence in the plane of the normal and the line as in Fig. 10 from FEKO method of moments modeling. The spike results from the twists of the strands. For the seven-strand line, this RCS spike should appear at about 10° from normal incidence according to Fig. 10. An Xpatch calculation for our 6.4-m cable, as shown in Fig. 11, shows the same spike. Another paper coauthored by Sarabandi[9] shows a measured RCS for a 30-cm-long, 7-strand cable at 34.5 GHz with a 1-GHz bandwidth, which is in reasonable agreement with our Xpatch result in Fig. 11 considering our narrower bandwidth and longer cable length.

Figures 21 through 24 for the 79.6° incidence show the strength of this RCS spike according to our SAR modeling. Consistent with the expectation, the peak return for the 79.6° incidence is about 30 dB higher in both the ParaView and Catalus images than at nearby azimuthal incidences of 84.6° or 74.6° Notably in our SAR images these latter two incidences show images or returns from the cable so weak that they are difficult to discern from the background noise or clutter.

3.2 ZSU Antiaircraft Vehicle

Figures 29 through 50 show Catalus and ParaView images of a ZSU antiaircraft vehicle at radar incidences of 90°, 60°, 30°, and 0° from the front of the ZSU, which is aligned with the X-axis. The exception is Fig. 34, which illustrates, as an example, the 60° incidence case of the radar direction relative to the ZSU orientation. Most of the images contain an overlay of the facet model or an outline of it.

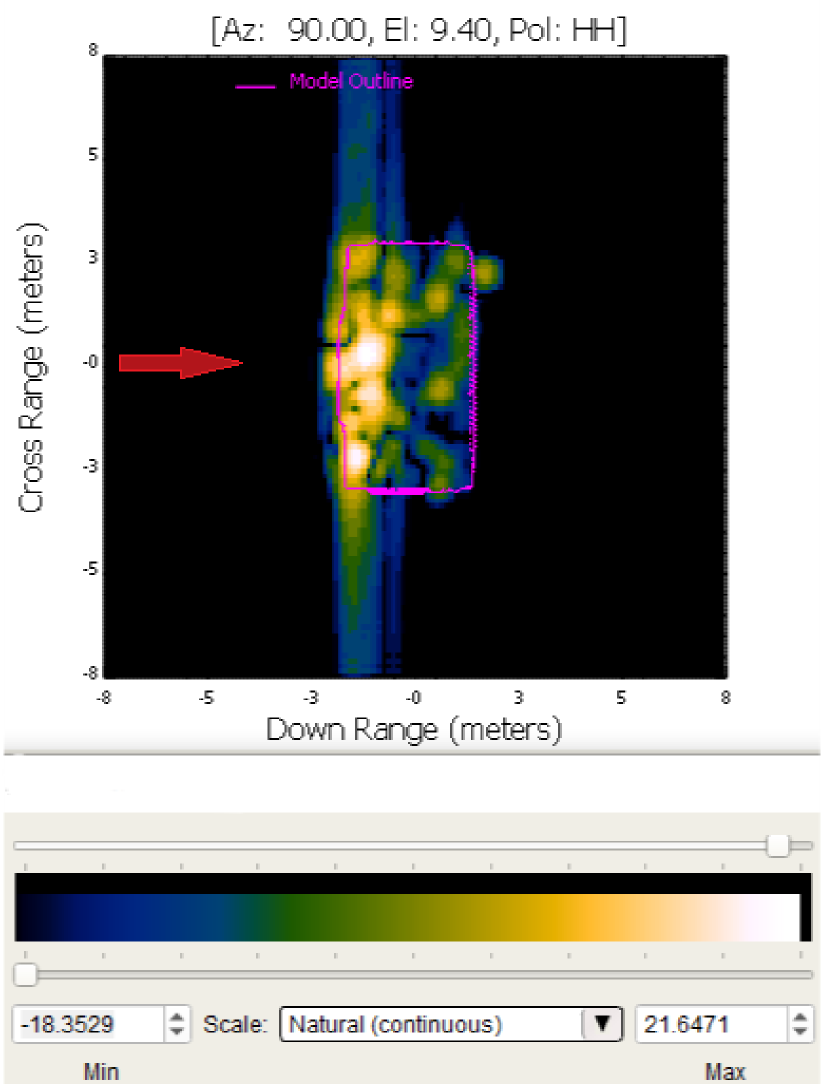

Fig. 29 Catalus free-space HH SAR (dB), broadside-inc against ZSU

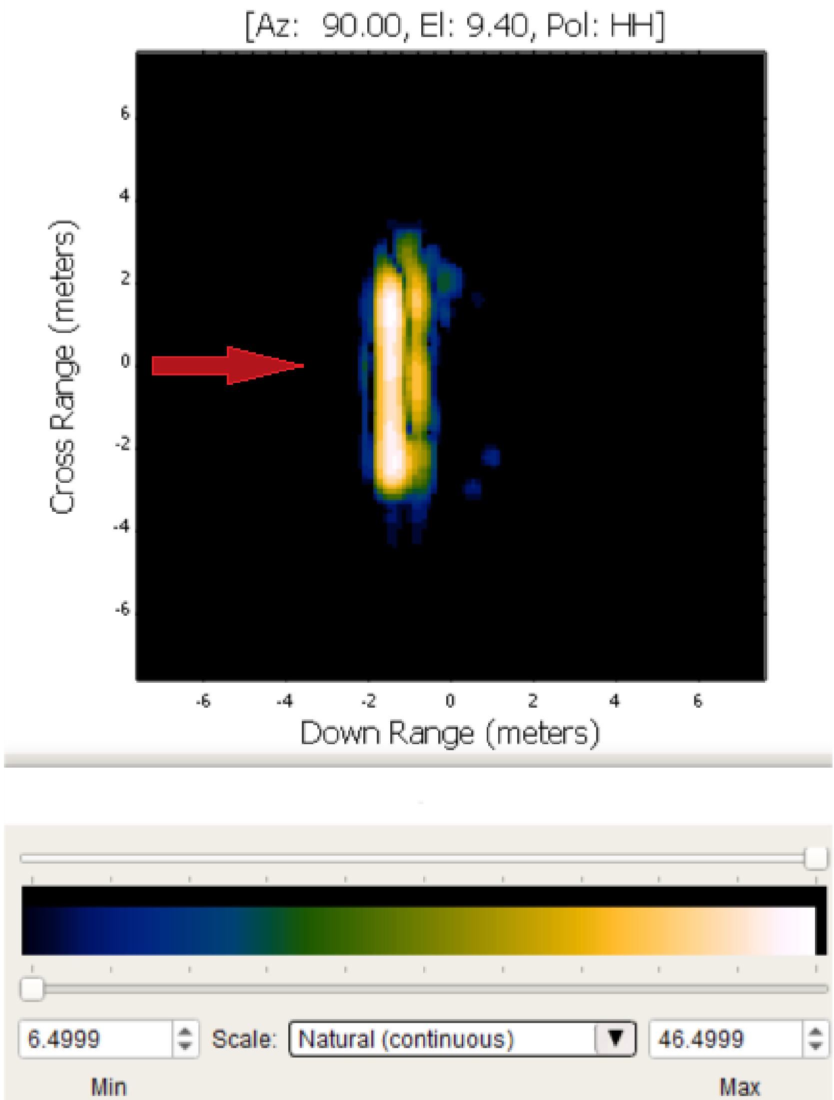

Fig. 30 Catalus HH SAR (dB) broadside-inc against ZSU over flat ground

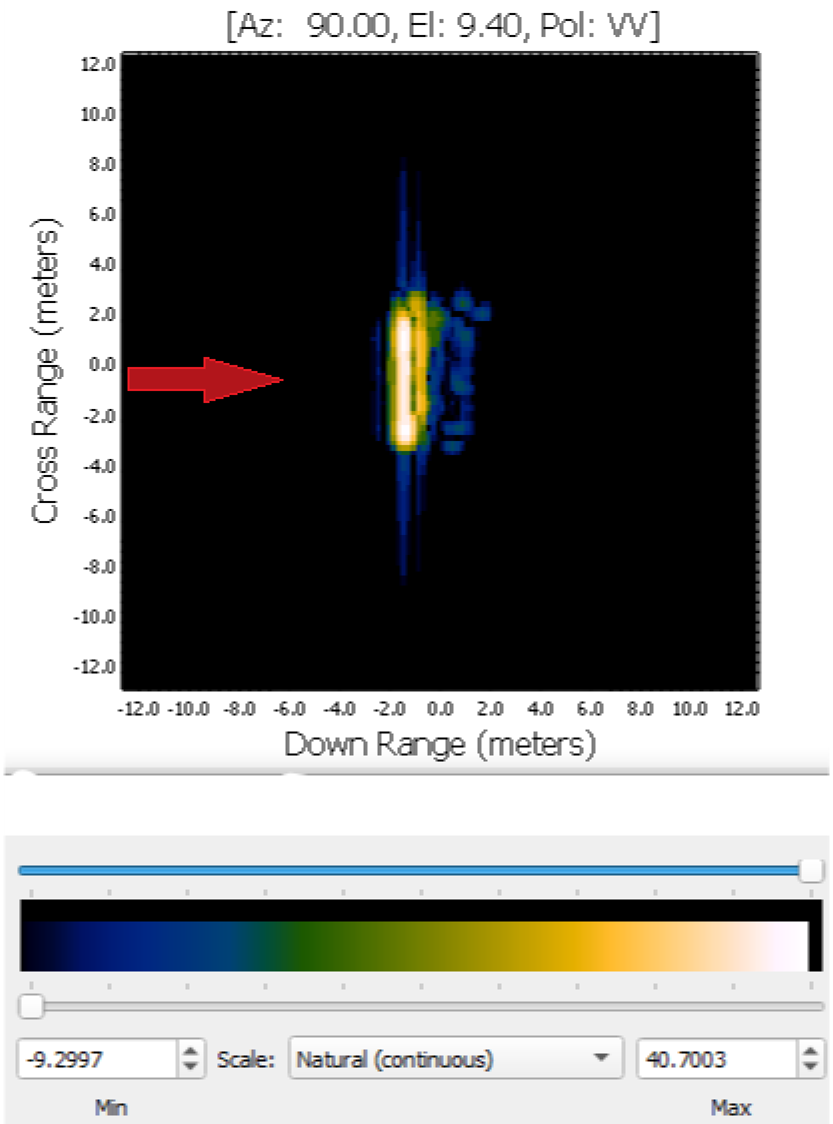

Fig. 31 Catalus VV SAR (dB) broadside-inc against ZSU over flat ground

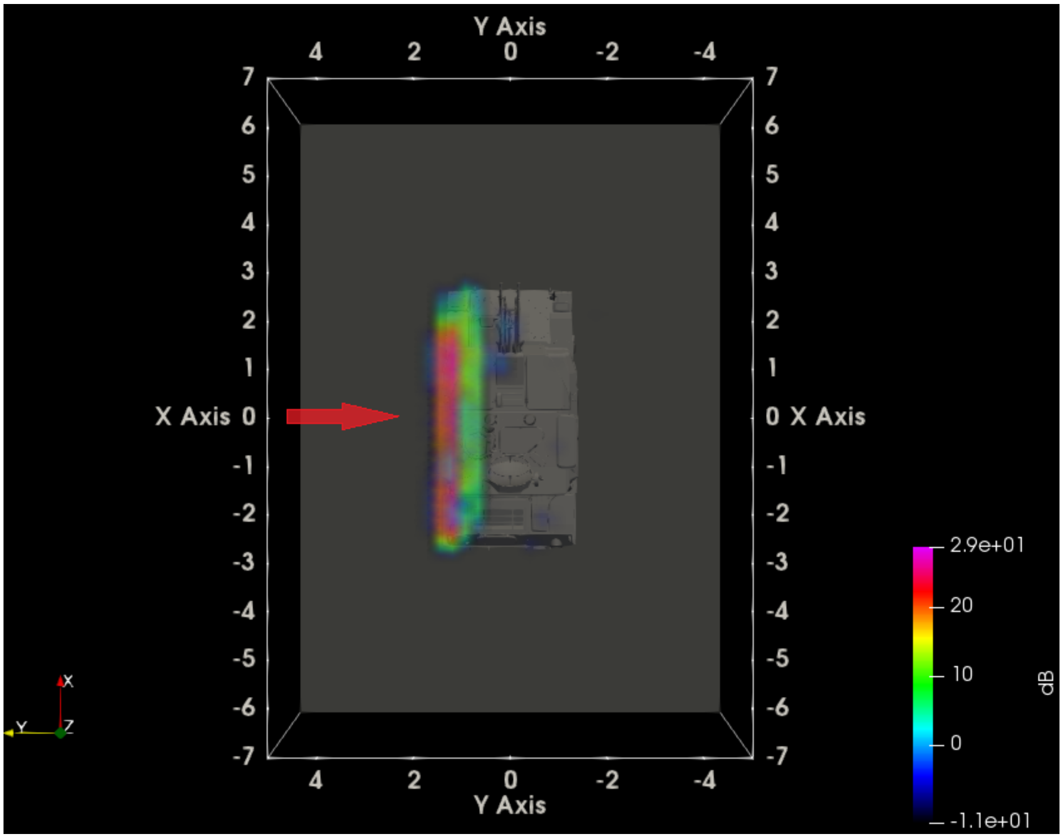

Fig. 32 ParaView HH SAR broadside-inc against ZSU over ground, top-down view

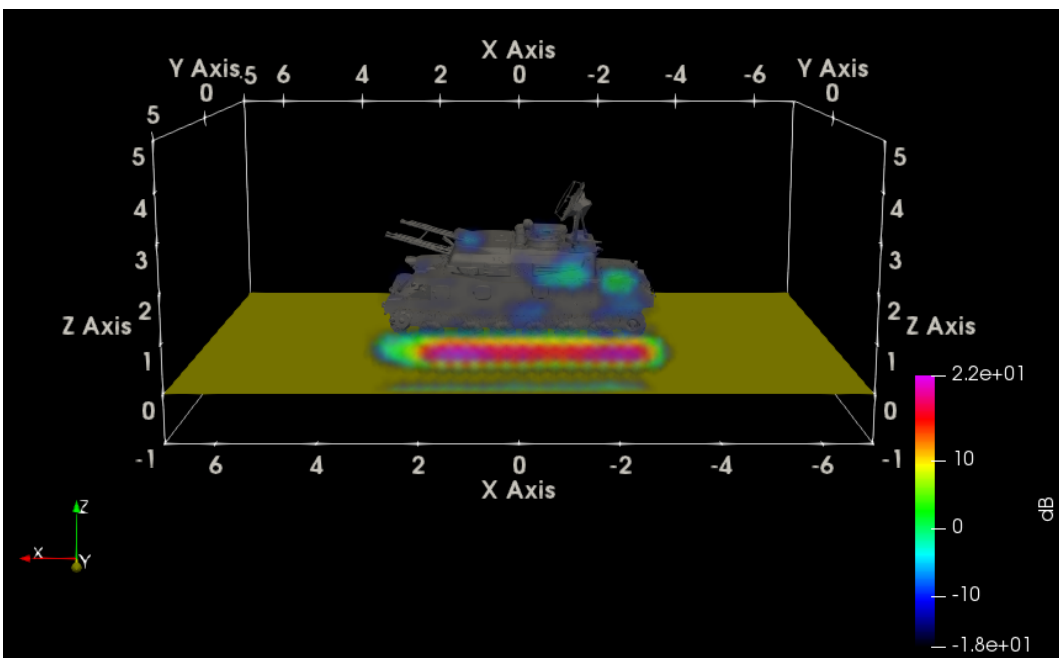

Fig. 33 ParaView VV SAR, broadside-inc on ZSU, radar view

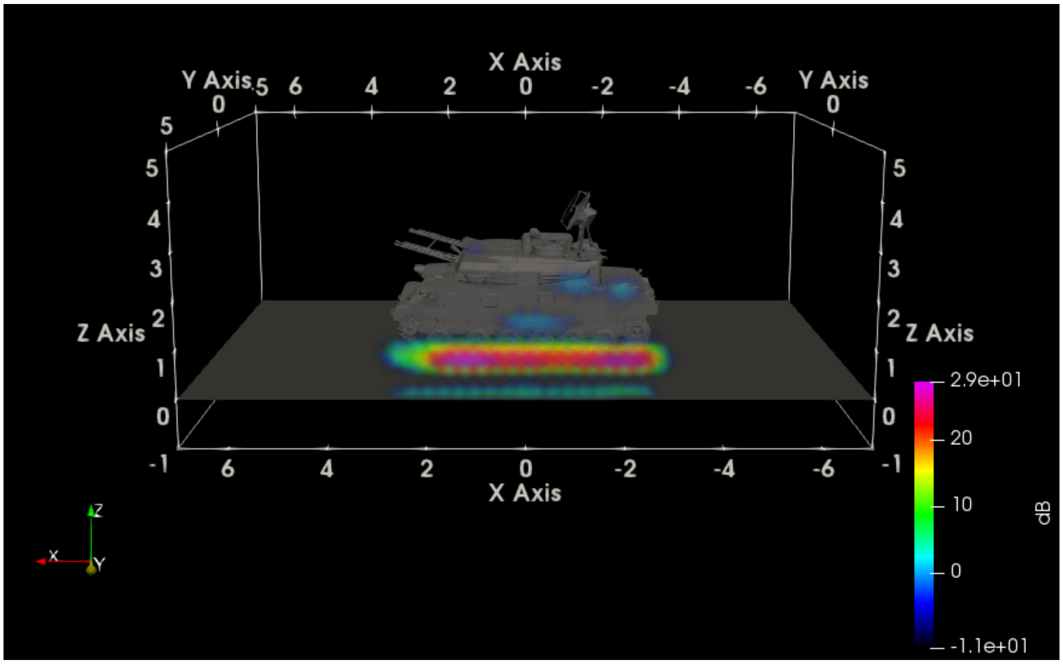

Fig. 34 ParaView HH SAR (dB), broadside-inc against ZSU, radar view

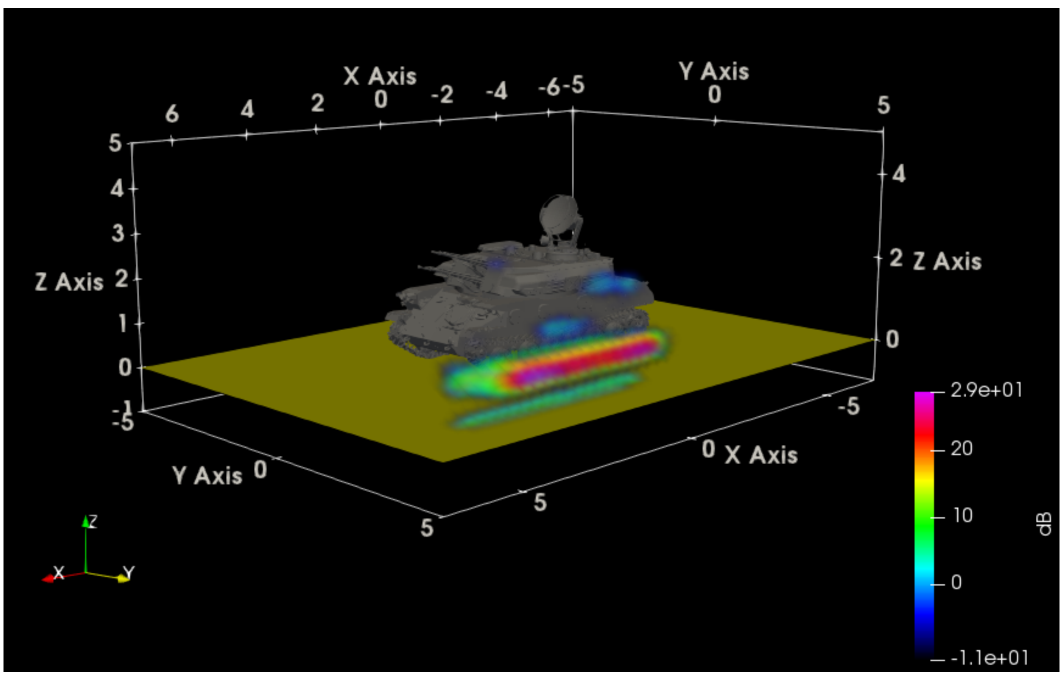

Fig. 35 ParaView HH broadside-inc, view turned 45°

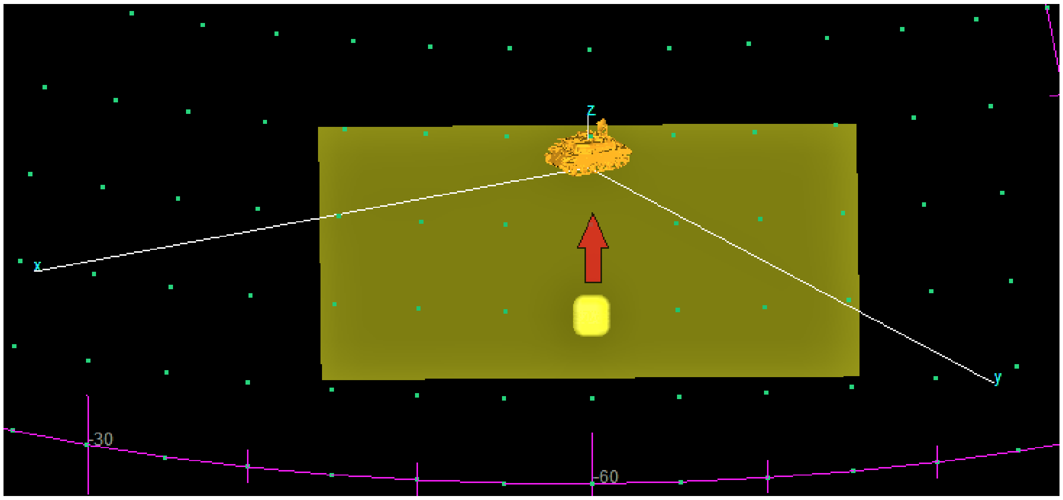

Fig. 36 ZSU at 60° radar azimuth-inc indicated by the yellow spot that spans the θ and φ angles of the radar apertures

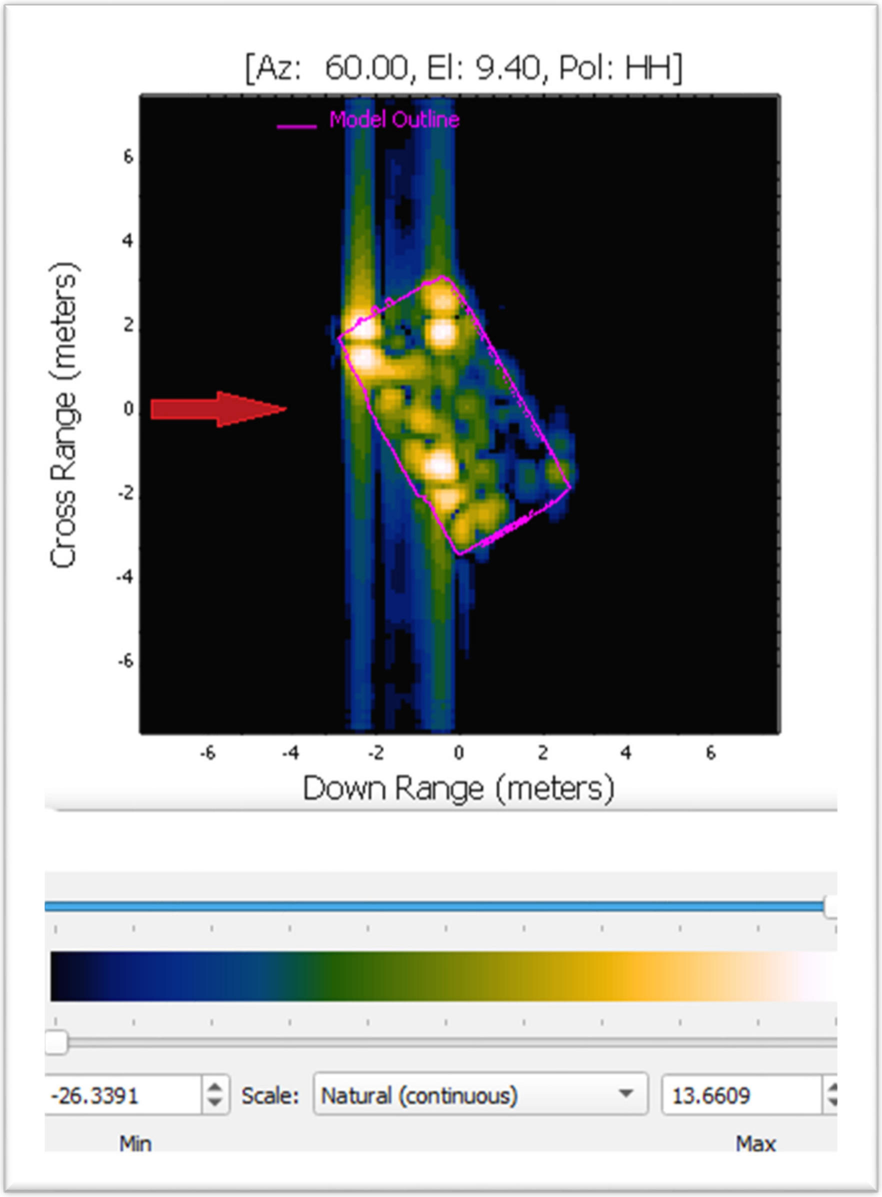

Fig. 37 Catalus HH 60° incidence (dB) on ZSU over flat ground with incidence from the left

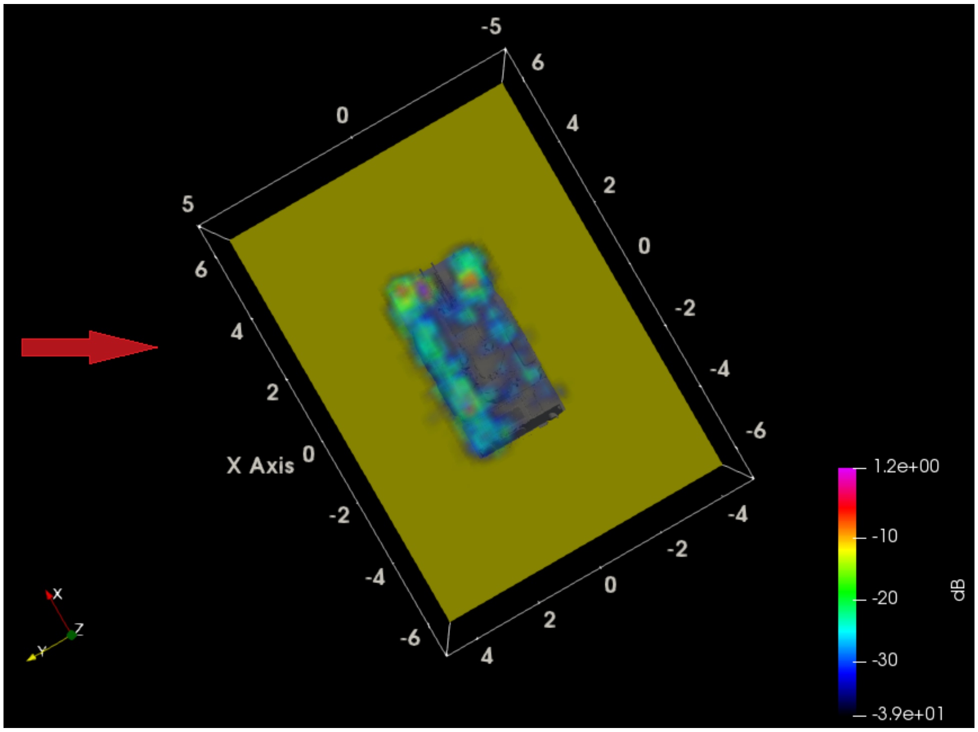

Fig. 38 ParaView HH 60° incidence on ZSU over flat ground, top-down view with incidence from the left

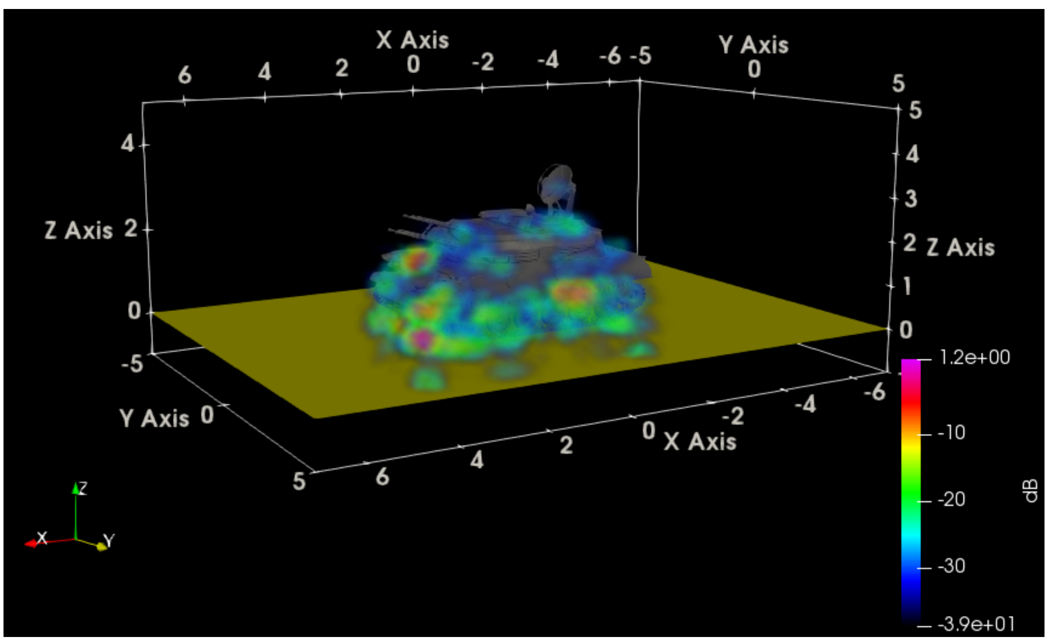

Fig. 39 ParaView HH SAR; 60° azimuth-inc (dB) on ZSU over flat ground, radar view

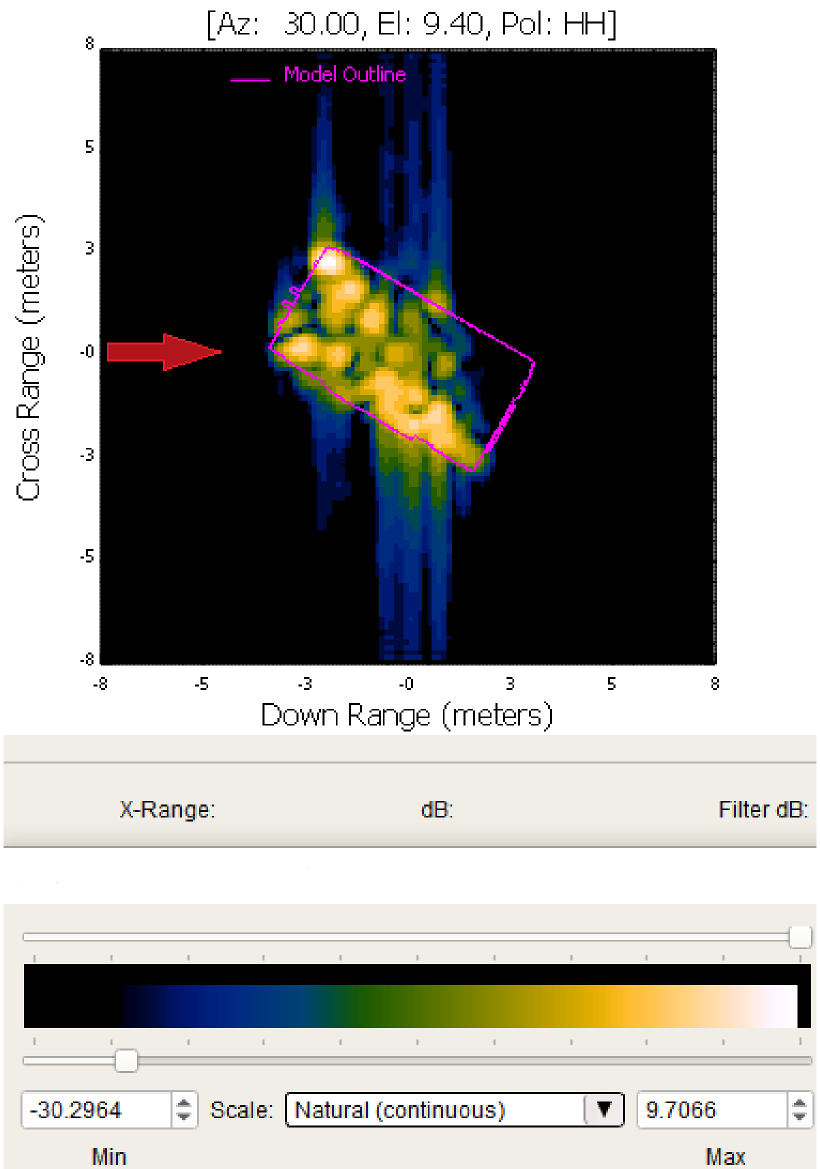

Fig. 40 Catalus HH SAR image of free-space ZSU; azimuth-inc at 30° (radar from the left)

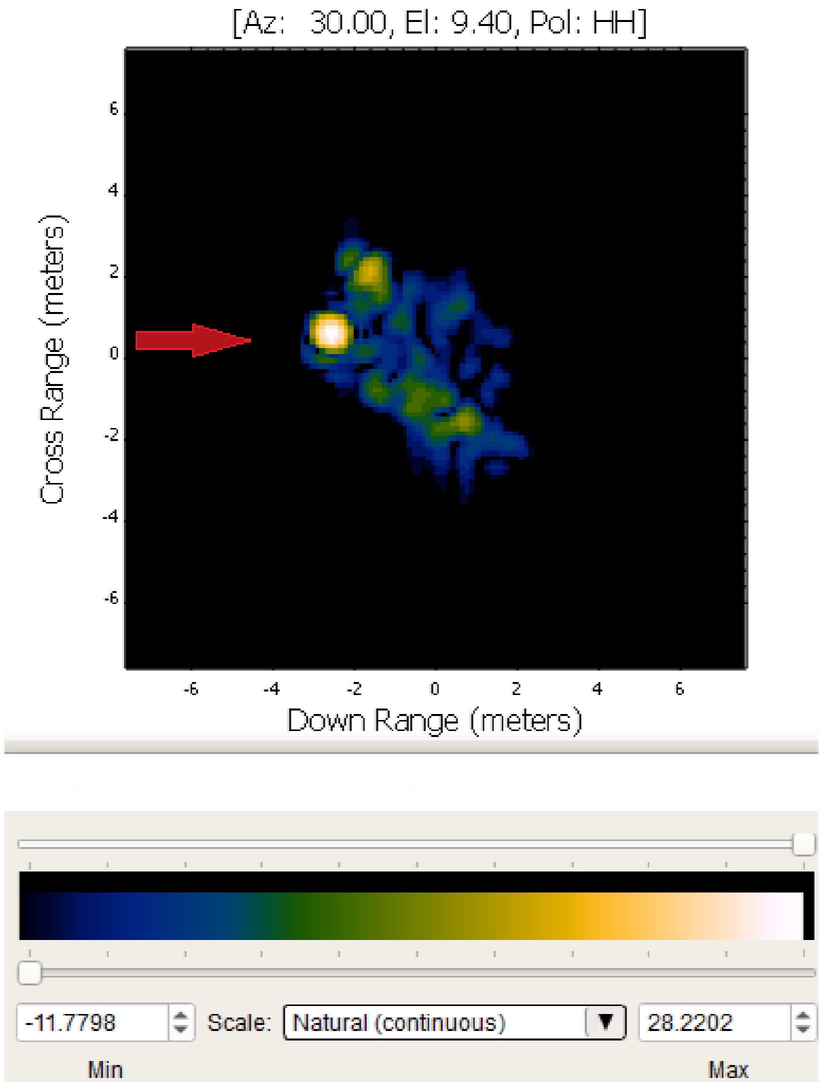

Fig. 41 Catalus HH SAR image (dB) of ZSU over ground; azimuth-inc at 30° (radar from the left)

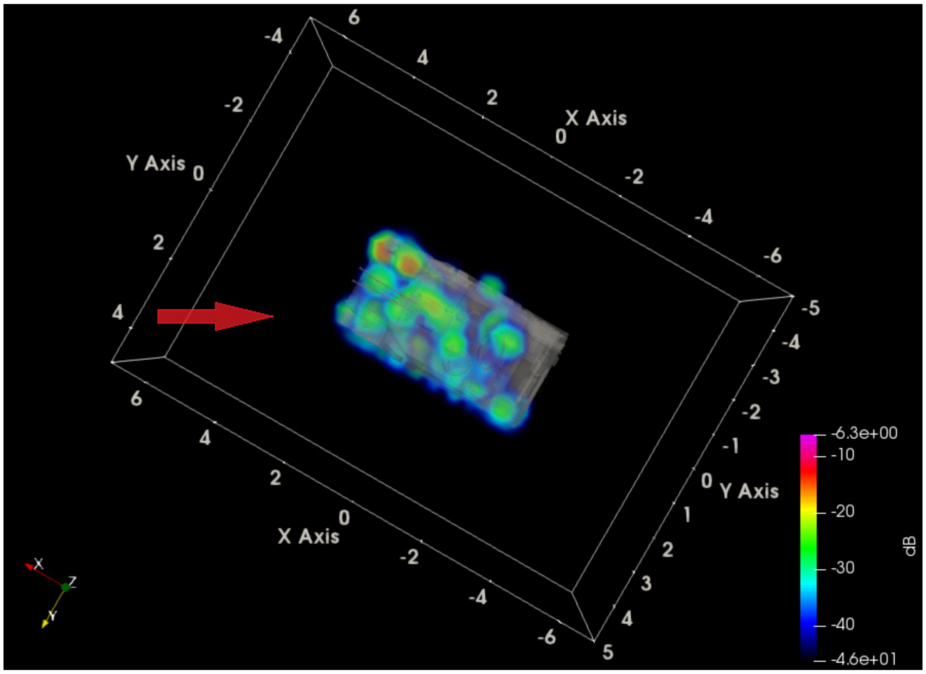

Fig. 42 ParaView HH SAR for 30° azimuth-inc on ZSU in free space, top-down view

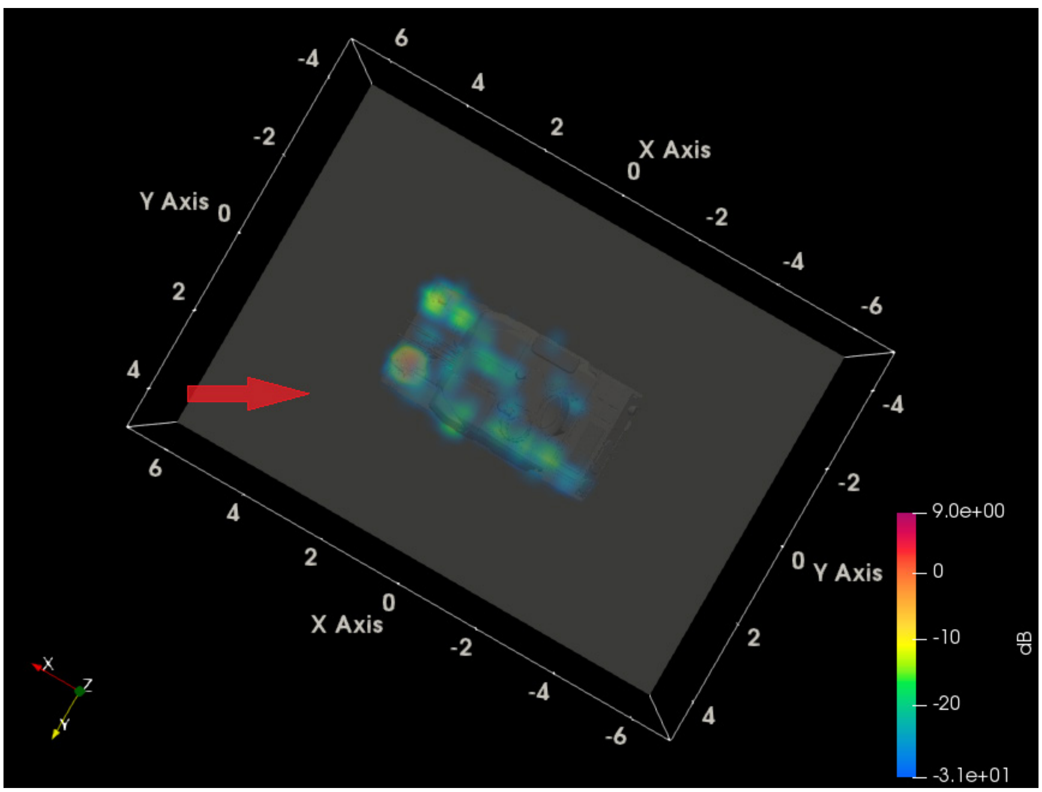

Fig. 43 ParaView HH SAR for 30° azimuth-inc on ZSU over ground, top-down view

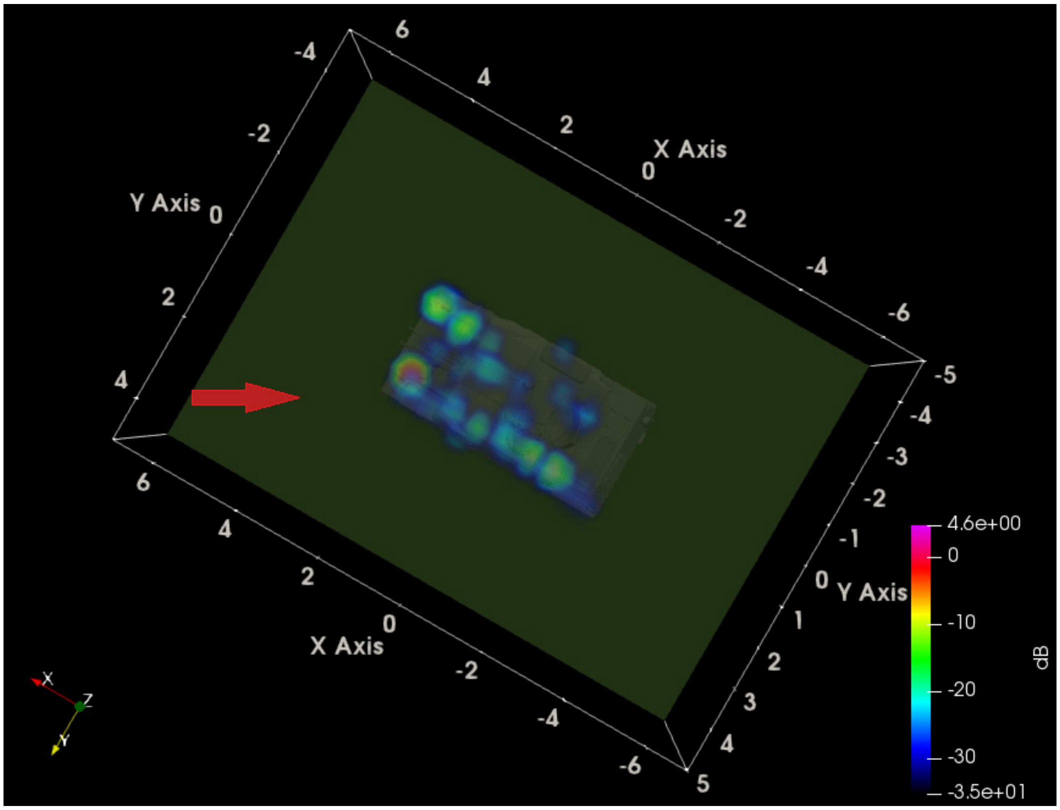

Fig. 44 **ParaView VV SAR for 30° azimuth-inc on ZSU over ground, top-down view**

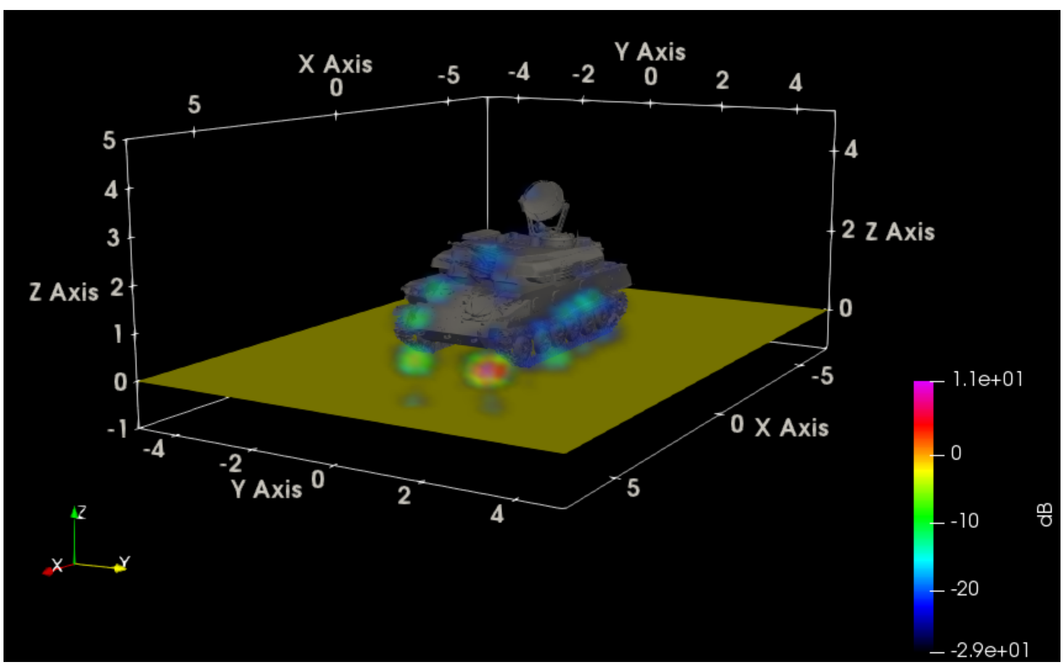

Fig. 45 **ParaView HH SAR for 30° azimuth-inc on ZSU, radar view**

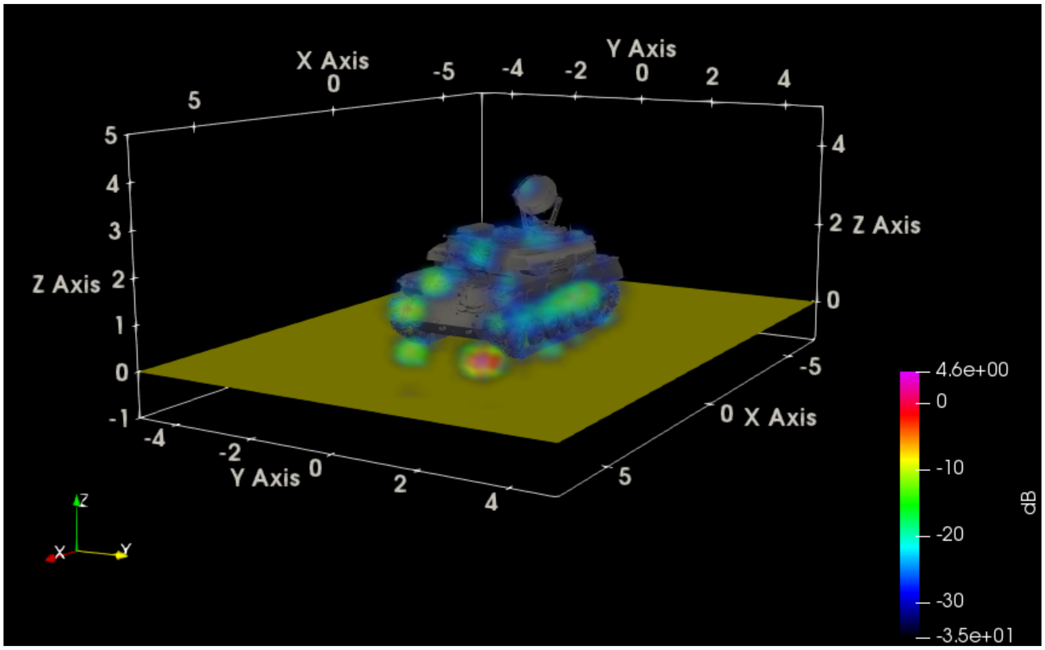

Fig. 46 ParaView VV SAR for 30° azimuth-inc on ZSU, radar view

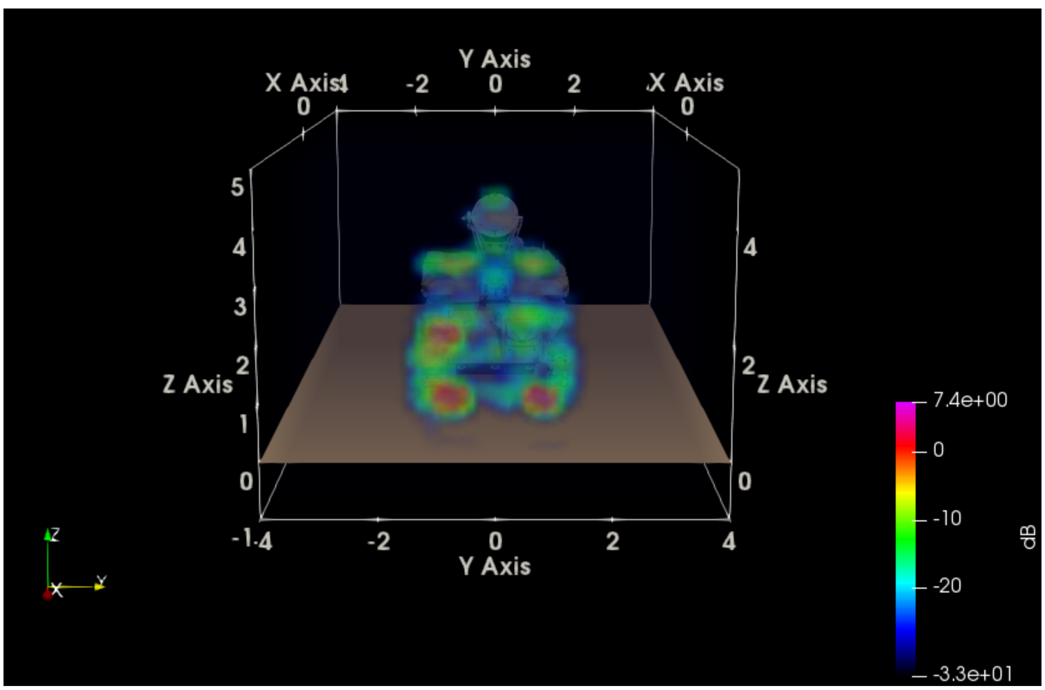

Fig. 47 ParaView VV SAR for 0° azimuth-inc on ZSU, radar view

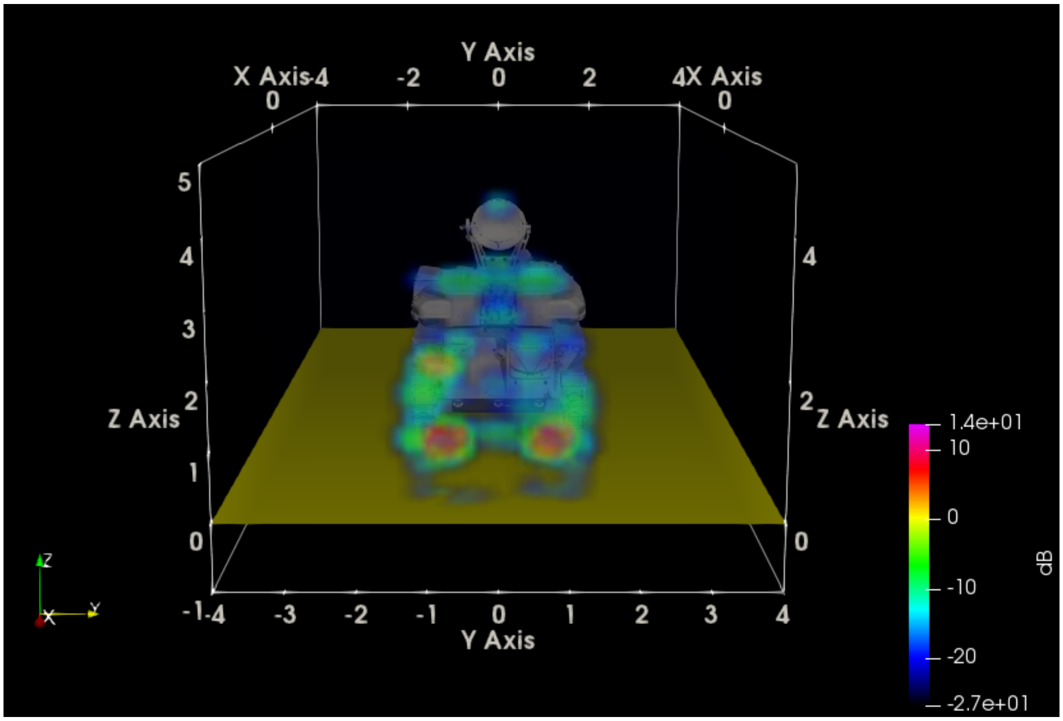

Fig. 48 ParaView HH SAR for 0° azimuth-inc on ZSU, radar view

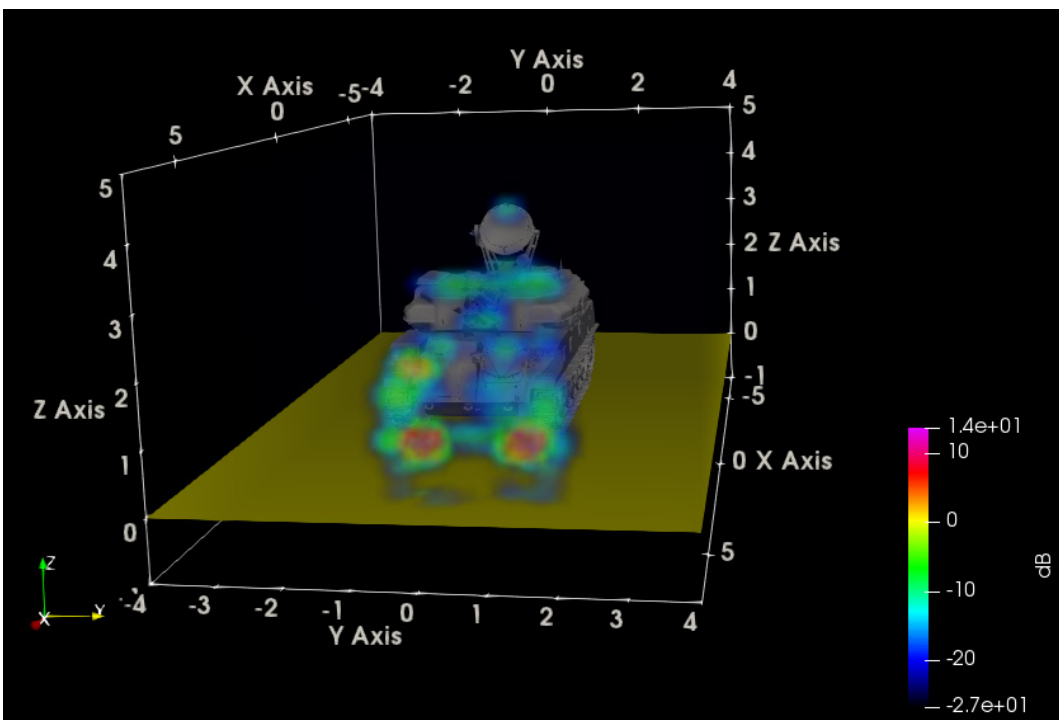

Fig. 49 ParaView HH SAR for 0° azimuth-inc on ZSU, 10° in azimuth from radar view

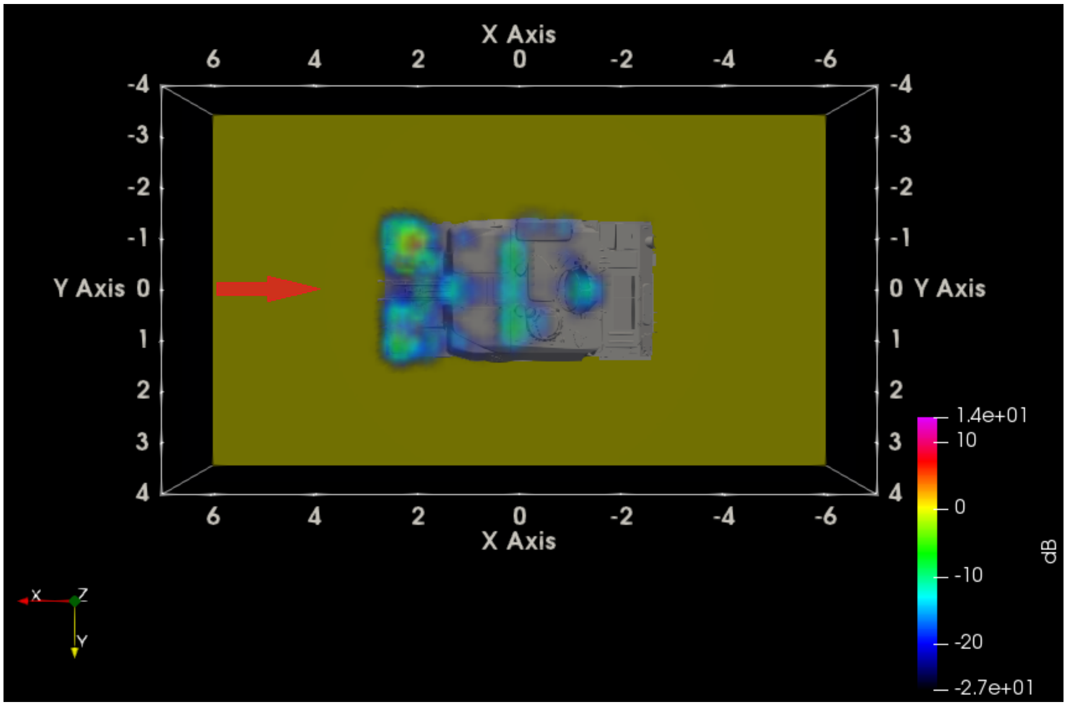

Fig. 50 ParaView HH SAR for 0° incidence on ZSU, top-down view (radar from the right)

Notably, the HH returns for this model are significantly stronger than the VV. For the broadside or 90° incidence, the former peak is 5 dB stronger in the 2-D SAR and 7 dB stronger in the 3-D SAR. Similarly, for frontal incidence on the ZSU, the HH peak return is 7 dB stronger than the VV peak return in the 3-D SAR. In the 2-D SAR the free-space HH SAR is 25 dB lower, showing that the ground interaction strongly enhances the return. Nevertheless, the pristine character of the model may overstate the relative strength of returns from certain sectors such as the tracks.

The returns for the ZSU, here, show that nearly all the returns are from the body, especially from the track regions, while few, if any, come from the guns or the dish antenna. This suggests that other tracked vehicles will include major returns from the body, and especially the tracks.

3.3 Boulder Field

The third principal target that we modeled was a boulder field of five boulders with three different sizes and shapes. Figure 7 in Section 2.2 showed the locations of the boulders over the field and Fig. 51 shows boulders as they could be seen optically from an approaching helicopter assuming that the field was not visually degraded. Figures 52 and 53 show SAR images for both the VV and HH polarizations cases as would be seen from the 3-D point of view of the radar. All boulders are clearly visible with returns stronger for larger boulders. The HH SAR returns are significantly stronger, as well.

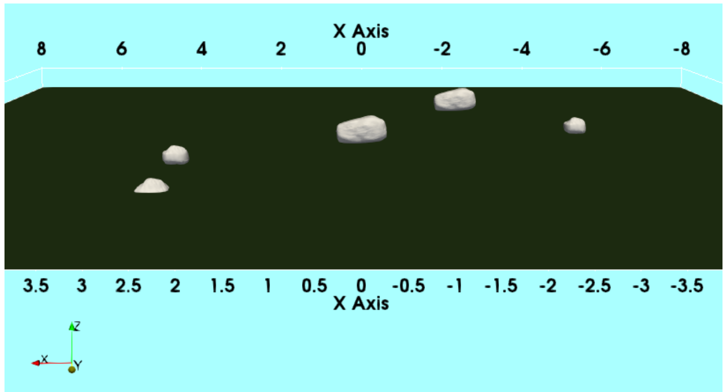

Fig. 51 Boulder field as viewed optically from approaching helicopter

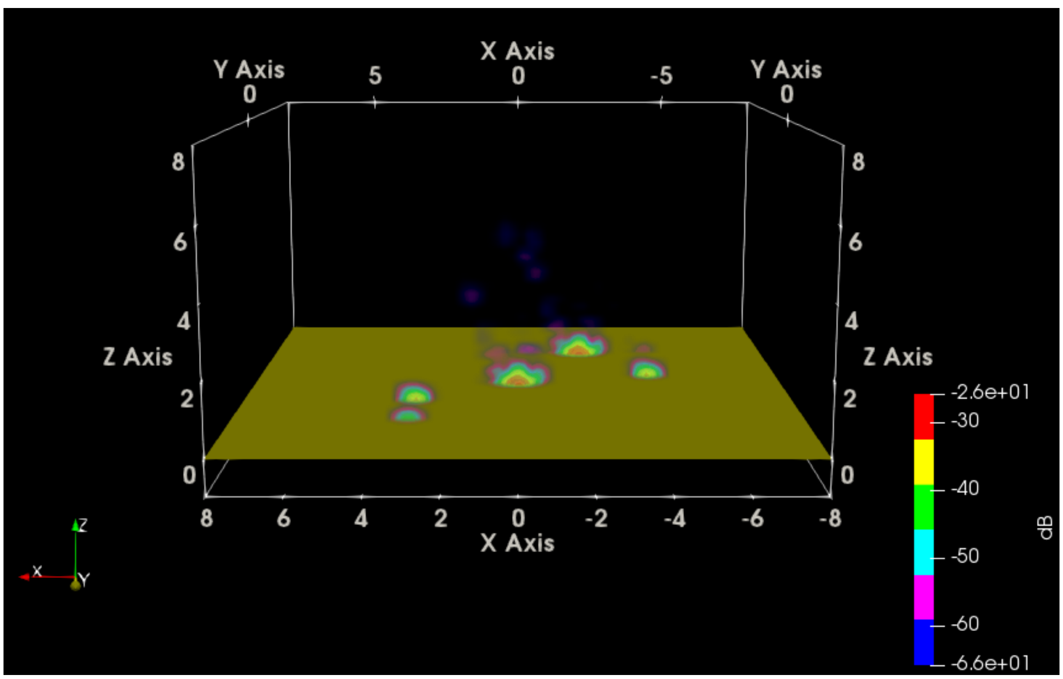

Fig. 52 ParaView HH SAR of boulder field, radar view

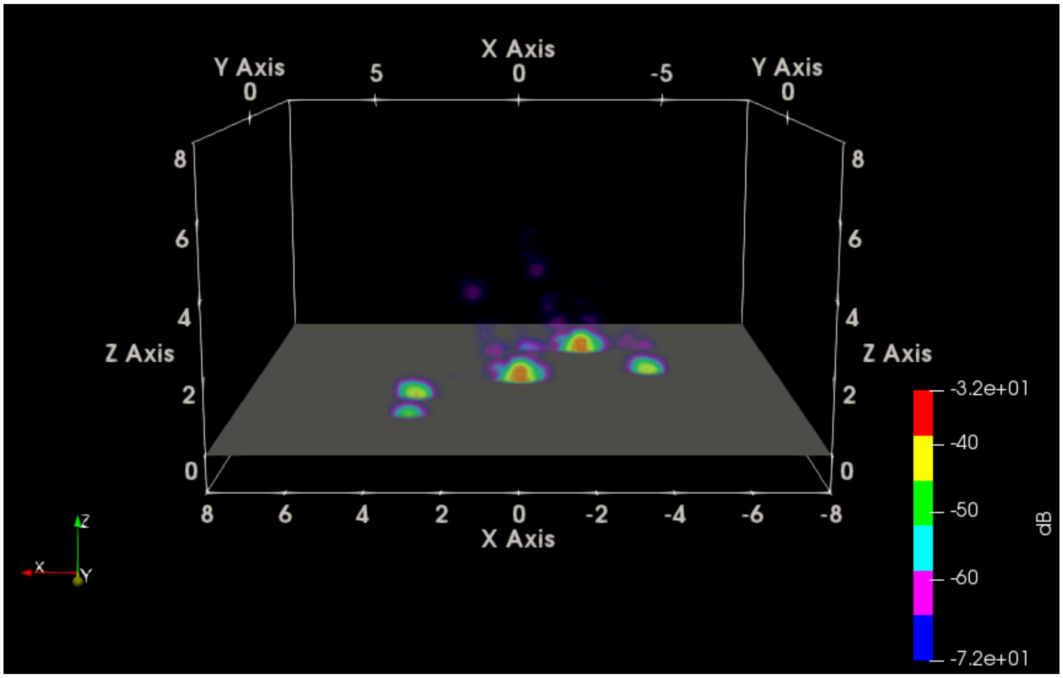

Fig. 53 ParaView VV SAR of boulder field, radar view

Figure 54 features a ParaView top-down view with boulder models that are shown bubble-like overlaying their respective VV SAR return hotspots. The SAR hotspots coincide very well with the boulder faces aimed at by the radar beam.

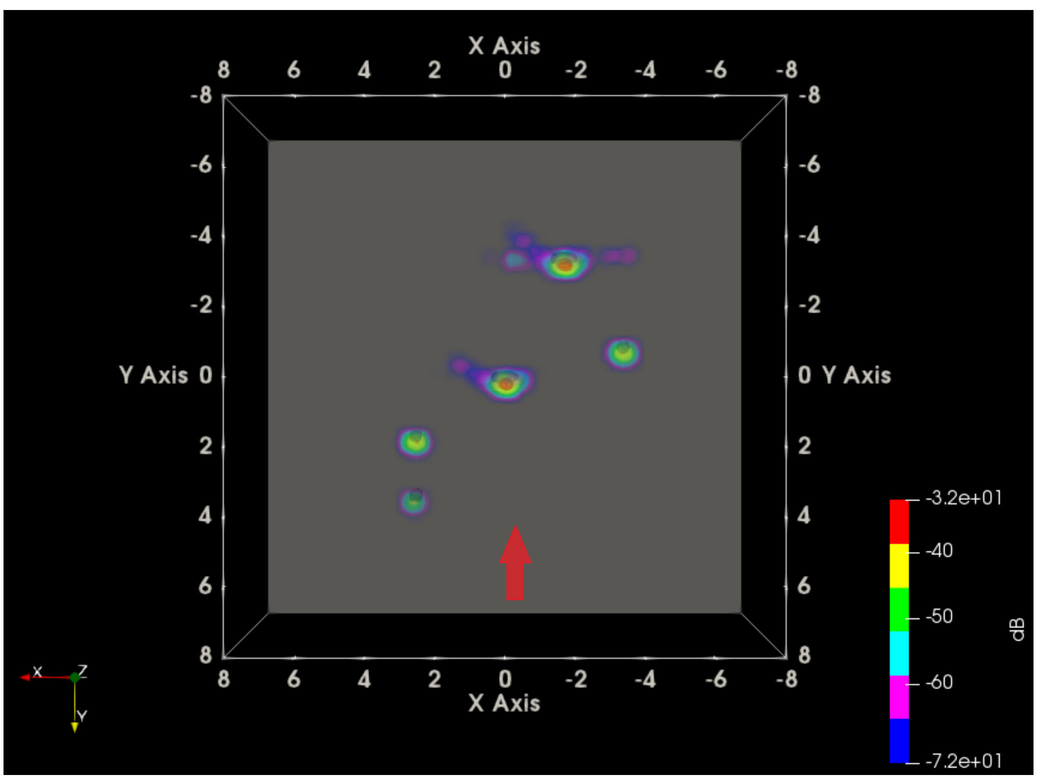

Fig. 54 ParaView VV SAR top-down view with boulders overlaid (bubble-like)

Figures 55 and 56, respectively, show the Catalus HH and VV 2-D SAR images for the boulder field. Catalus has a feature allowing display of SAR magnitudes at user-selected points within the image. Using this tool, we compared peak returns of each the boulders with the peak return of the 0.5-m free-space PEC sphere of Fig. 9. The peak 2-D SAR return for the PEC sphere is –12.2 dB.

In Fig. 55, we have labeled the boulder images as follows: 1 is for the 19-inch boulder, 2 and 3 are the 16-inch boulders, and 4 and 5 are the 36-inch boulders. The peak 2-D HH return for 1 is –20.6 dB; for 2 and 3, it is –16.6 dB; and for 4 and 5, it is –6.5 dB. The free-space PEC sphere 2-D peak SAR return falls roughly in the middle of the boulder returns.

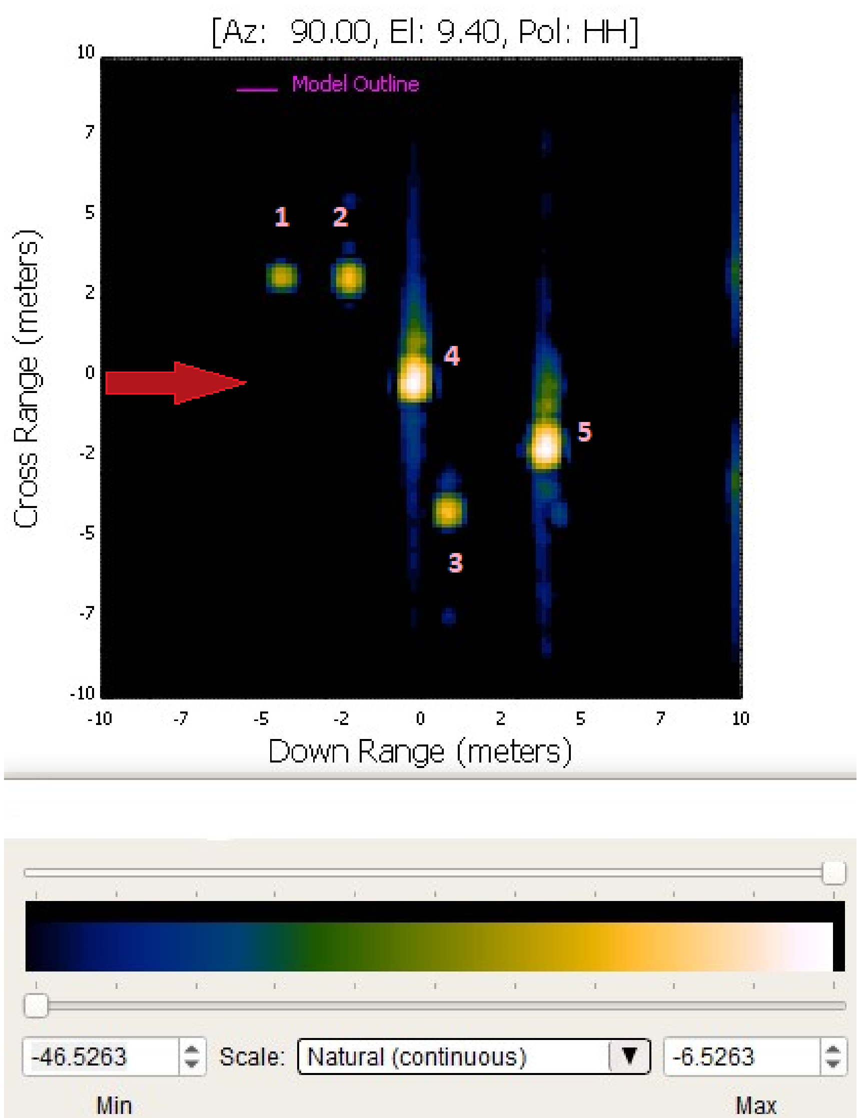

Fig. 55 Catalus HH SAR of boulder field over ground

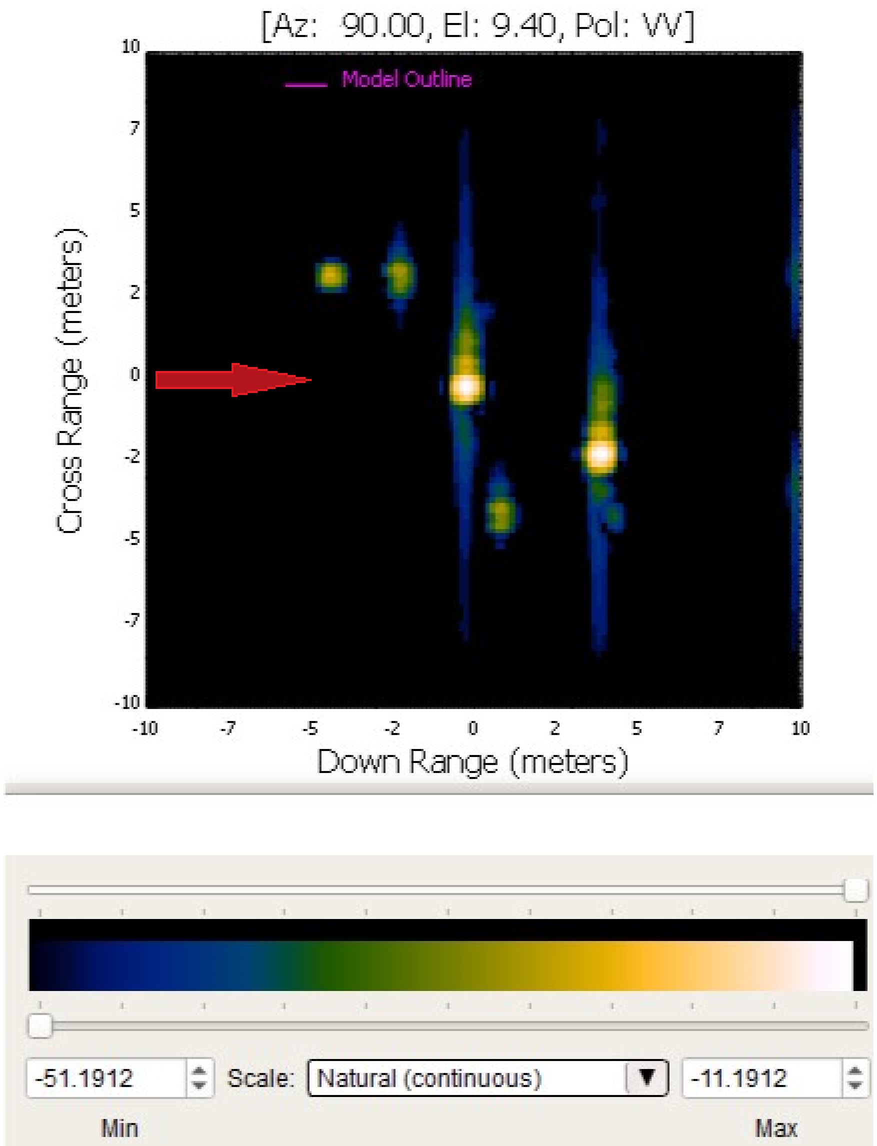

Fig. 56 Catalus VV SAR of boulder field over ground

Figures 57 through 64 are ParaView SAR images of the boulder field as viewed from the radar with increasing ground roughness. The roughness is characterized by the RMS height and correlation length of its collection of bumps of various heights. We have kept the correlation length for every rough ground at 2 m, but have varied the RMS height of the Xpatch-generated random bumps as we created each ground plane. The hypothesis here is that if the ground becomes sufficiently rough by increasing the RMS height of its bumps, the resultant radar clutter will begin to adversely affect the radar image quality and eventually obscure the targets we are trying to see using the radar.

What we do see over this range of ground roughness is that the peak returns decline by several decibels as we go from 1 to 15 cm in RMS height. This would make sense as the increased ground scattering would cause ground bounces to diverge rather than enhance the principal images. Also a few more artifacts or distortions appear in the images, though not so much as to obscure the main images.

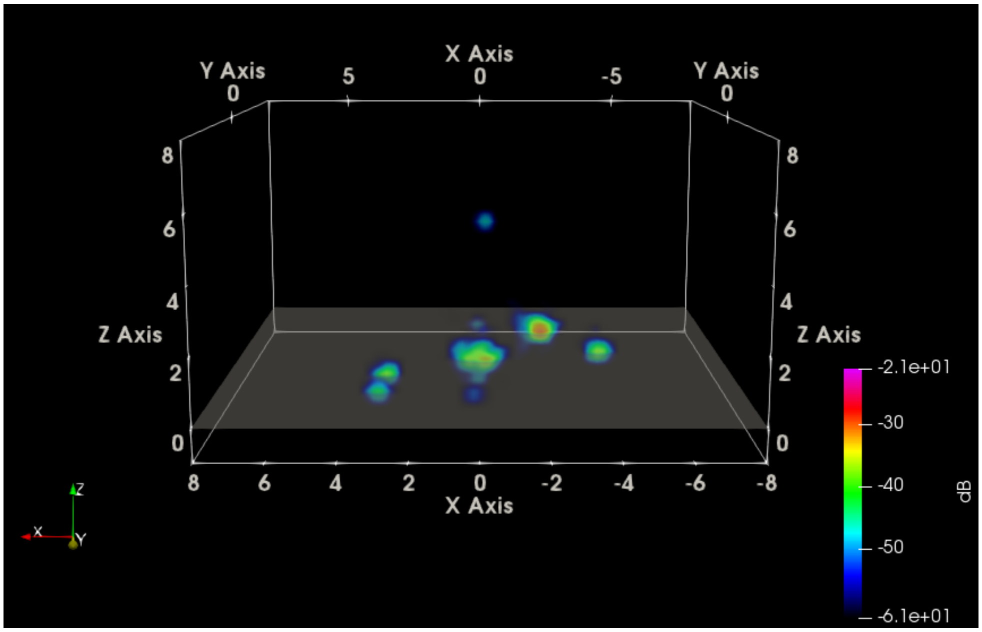

Fig. 57 Radar-view HH SAR of five boulders with rough ground RMS bump height = 1 cm

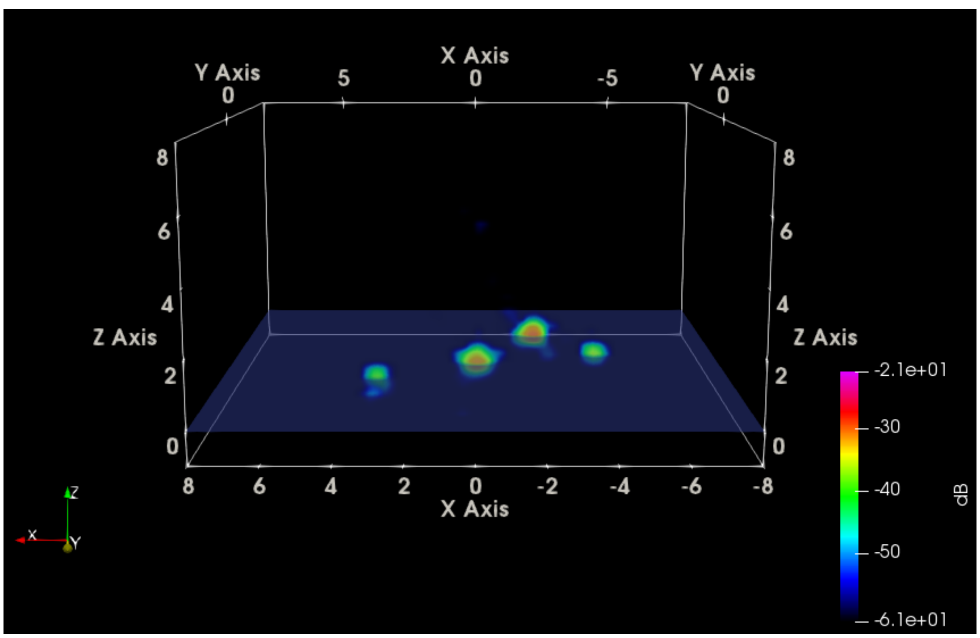

Fig. 58 Radar-view HH SAR of five boulders with rough ground RMS bump height = 3 cm

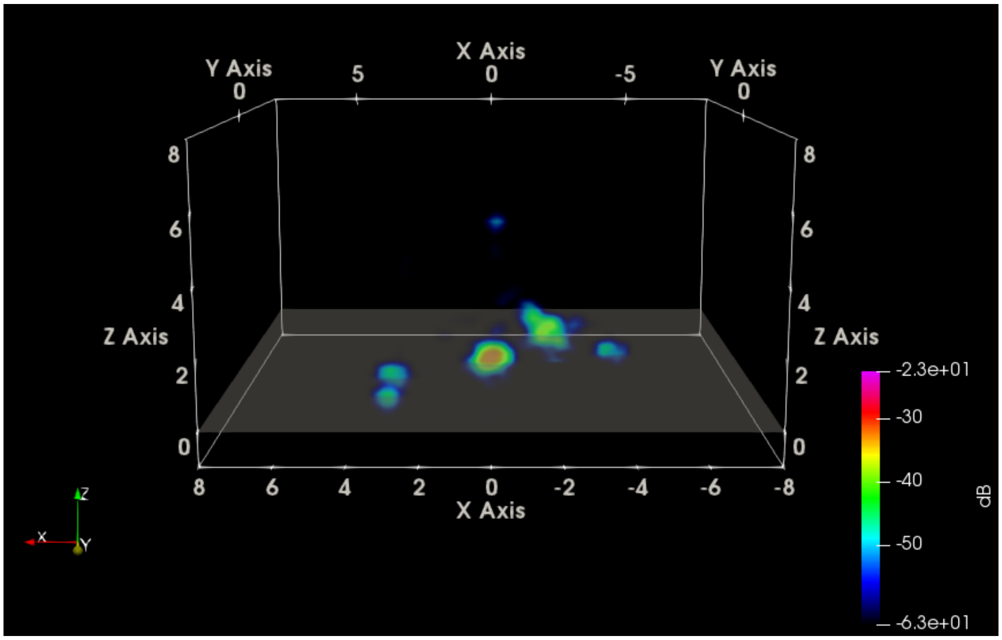

Fig. 59 Radar-view HH SAR of five boulders with rough ground RMS bump height = 6 cm

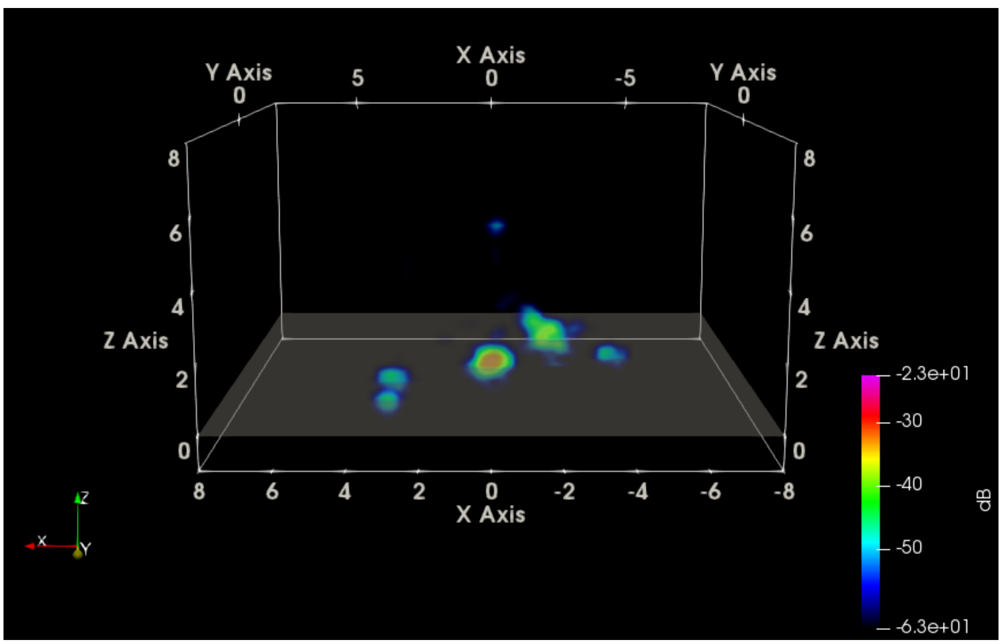

Fig. 60 Radar-view HH SAR of five boulders with rough ground RMS bump height = 10 cm

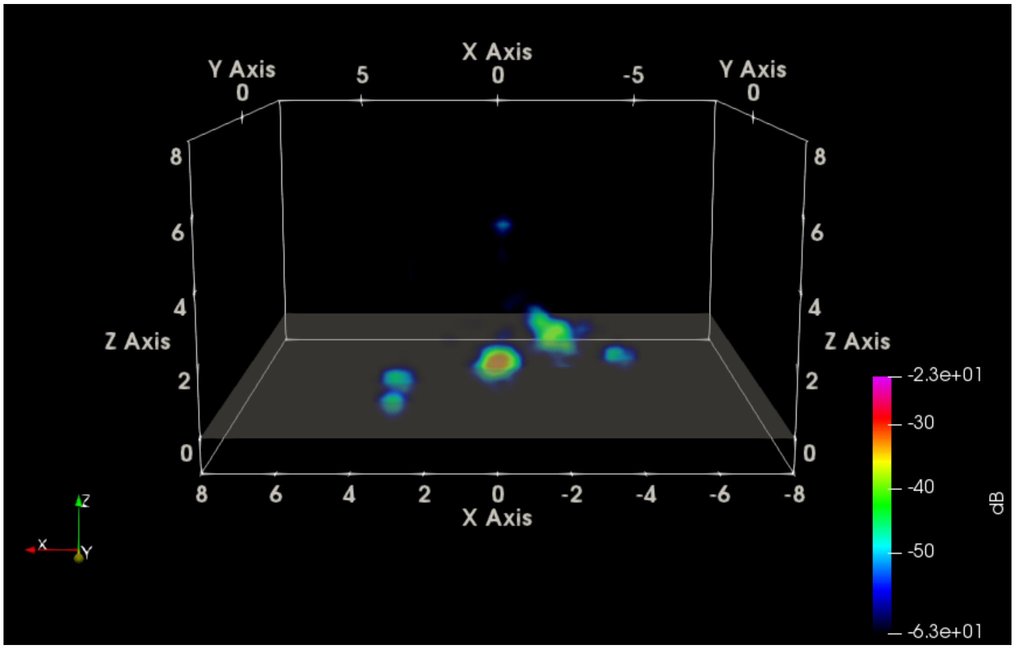

Fig. 61 Radar-view VV SAR of five boulders with rough ground RMS bump height = 3 cm

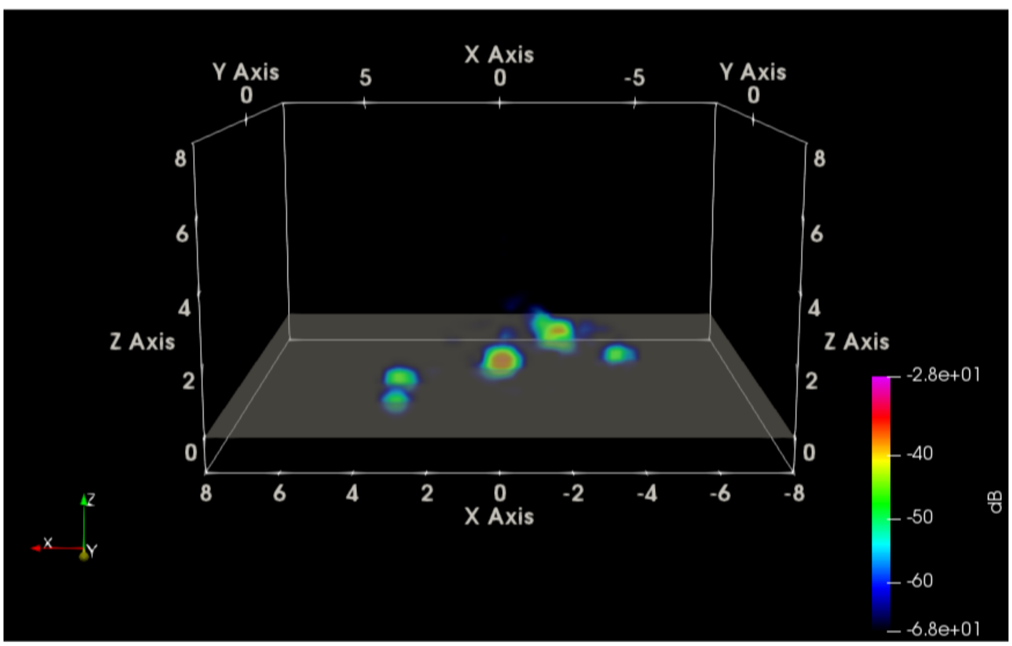

Fig. 62 Radar-view VV SAR of five boulders with rough ground RMS bump height = 10 cm

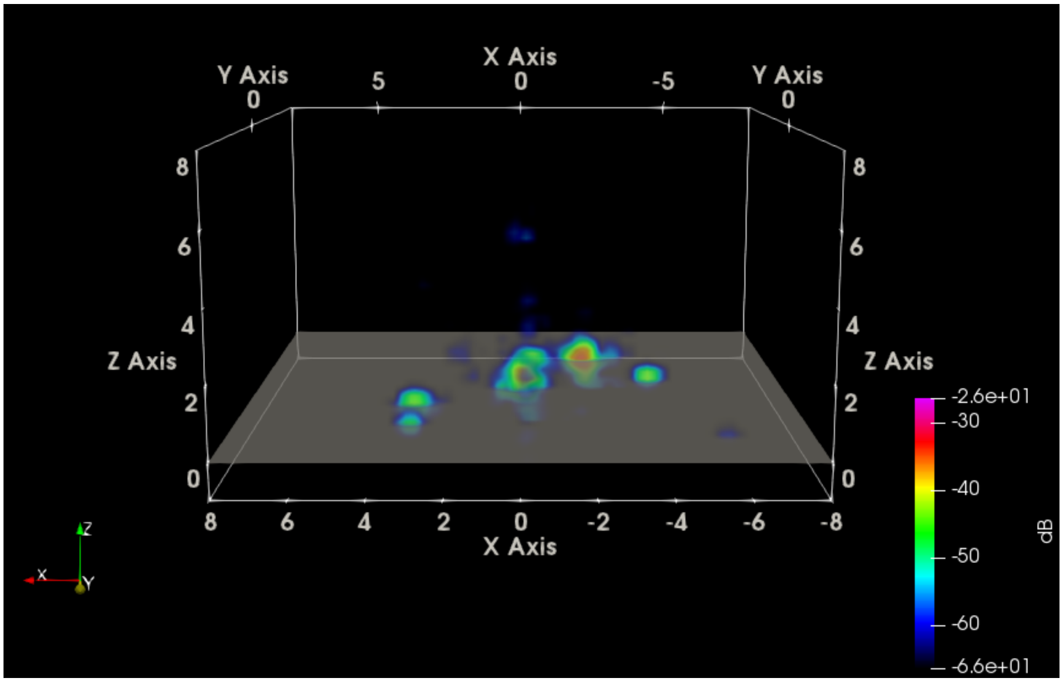

Fig. 63 Radar-view HH SAR of five boulders with rough ground RMS bump height = 15 cm

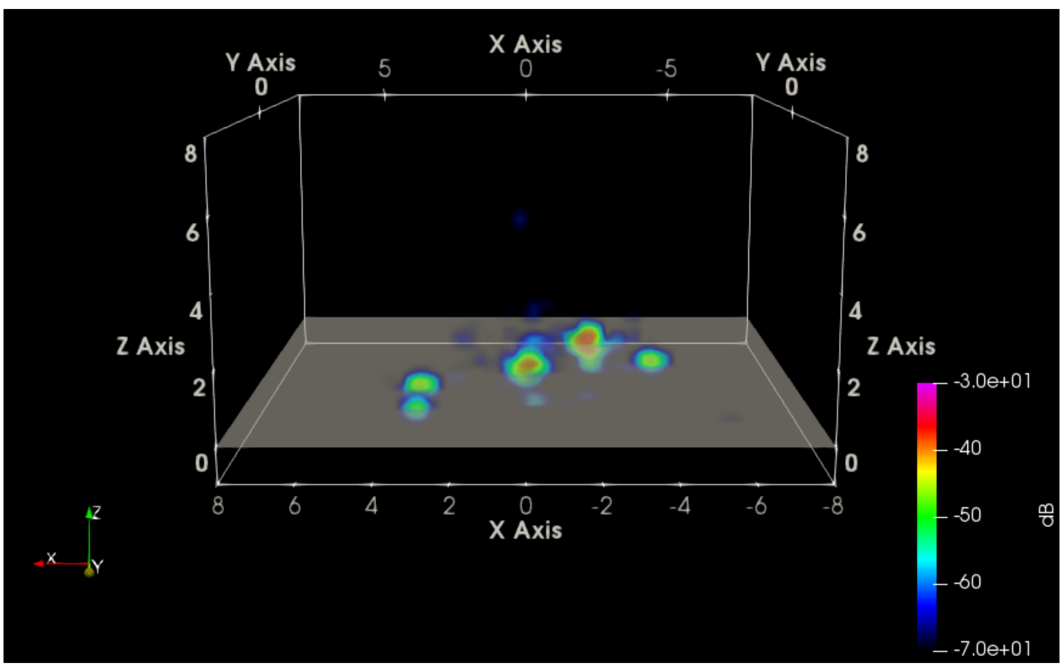

Fig. 64 Radar-view VV SAR of five boulders with rough ground RMS bump height = 15 cm

4. Conclusions

Through computer modeling, we aimed to get an idea of what could be seen with a forward-looking 35-GHz helicopter landing radar. We have seen, especially from the 3-D ParaView images, that the location of an obstacle can be easily seen in the image boxes. Identifying smaller objects or their size appears to be more difficult than larger ones within the aperture and frequency bandwidth limitation of this possible radar.

Tracked vehicles can not only be seen, but probably can be identified at least as a tracked vehicle. Also, other metallic vehicles are likely to be seen based on the significant returns from the body of the ZSU exclusive of its tracks. Our pristine ZSU model may exaggerate some of the returns, as an actual ZSU will have imperfections from wear and tear, manufacturing tolerances, and differences due to positioning in a test setting.

In this study, most of our modeling was over a flat ground, with the exception of the boulders, which did include some results with rough ground. The boulders, varying in size horizontally from about 0.5 to 0.9 m and vertically from roughly 0.2 to 0.5 m, are clearly visible with only a little change in the image quality near the upper range of ground roughness, specifically with ground bump RMS heights varying from 1 to 15 cm at a fixed correlation length of 2 m. Also, that the boulders had the same permittivity as the ground did not render them too hard to see.

Our seven-strand power line can be seen, though possibly only at a few narrow incidence angle bands. Outside those angles, the power line may be difficult to distinguish from clutter. Yet the narrow visibility angle bands may hint at its identity.

The modeling in this report does not show cases for heavy clutter, as most of the modeling, except for several rough-ground boulder cases, was with a flat ground. Consequently, cases with more and heavier clutter need to be explored to capture more cases of what potential DVE landing zones may encompass. However, at least for the three cases of this report, the obstacles can be seen and usually stand out.

We have also tried to vary viewpoint and dynamic range as well as some other features in ParaView to see how images might be changed to better provide information to a pilot. ParaView 3-D images give a more intuitive sense of where an obstacle might be than the 2-D SAR images. When in 3-D mode, the 3-D sense especially comes through via small changes in camera or viewer perspective, not unlike how our eyes give us stereo vision or how we sense the depth through small changes in our transverse visual perspective of an object.

ParaView has the capability to export the 3-D images to VRML format, which, with the proper viewing hardware, could be an alternative way to view the 3-D images. Another way to provide vital information on the location of ground objects would be to grid the scene so that the pilot could see the locations of objects, relative to, say, 2-m marks. Of course, for a radar system, a design path to consider would be to take the same or other algorithms, with much the same result that we implicitly used with Matlab and ParaView, to generate the 3-D SAR images of actual obstacles for the pilot.

For this study, the biggest computational burden was the Xpatch generation of the 35-GHz radar data, which can take on the order of 10,000 CPU hours for a single look at a simple target over rough ground and hundreds of thousands or more for a wide sweep of incidence angles. However, for an aircraft, the radar is supplying that data, though after some conversion, and the remaining computational burden of a 3-D image might be like what Matlab does in roughly 30 min with five or six processors for a $51 \times 51 \times 51$ image space.

5. References

1. Dogaru T. Synthetic aperture radar for helicopter landing in degraded visual environments. Army Research Laboratory (US); 2018 Dec. Report No.: ARL-TR-8595.

2. Leidos. Xpatch. c2021. [accessed 2020 Sep]. https://www.leidos.com/products.

3. Chase R, Wallace BH, Blalock T. Numerical computation of the radar cross section of the ZSU-23-4. Army Research Laboratory (US); 1999 Apr. Report No.: ARL-MR-430.

4. Richards M, Scheer J, Holm W. Principles of modern radar, vol I. Scitech Publishing; 2010.

5. Altair Engineering, Inc. Altair FEKO. c2021 [accessed 2020 Sep]. https://altairhyperworks.com/product/Feko.

6. Sarabandi K, Park M. A radar cross-section model for power lines at millimeter-wave frequencies. IEEE Trans Antennas Propag. 2003 Sep;51(9).

7. Army Virtual Targets Center (US). Army Model Exchange. c2021 [accessed 2020 Sep]. https://modelexchange.army.mil.

8. Kitware Inc. ParaView website. c2021. [accessed 2020 Sep]. https://www.paraview.org/.

9. Sarabandi K, Pierce L, Oh Y, Ulaby FT, Power lines: radar measurements and detection algorithm for polarimetric SAR images. IEEE Trans Aerosp Electron Syst. 1994;30(2).

List of Symbols, Abbreviations, and Acronyms

1-D	one-dimensional
2-D	two-dimensional
3-D	three-dimensional
ARL	Army Research Laboratory
CAD	computer-aided design
CPU	central processing unit
DEVCOM	US Army Combat Capabilities Development Command
DVE	degraded visibility environment
HH	horizontal-horizontal
inc	incidence
PEC	perfect electric conductor
RCS	radar cross section
RMS	root mean square
ss	synthetic signal
SBR	shooting-and-bouncing ray
SAR	synthetic aperture radar
VV	vertical-vertical

1	DEFENSE TECHNICAL
(PDF)	INFORMATION CTR
	DTIC OCA
1	DEVCOM ARL
(PDF)	FCDD RLD DCI
	TECH LIB
1	DEVCOM ARL
(PDF)	FCDD RLS RM
	C KENYON